FABIO ARNALDO POMAR AVALOS

TIME SERIES ANALYSIS OF REMOTELY SENSED DATA AS A TOOL FOR VEGETATION EVALUATION AND SOIL-WATER INTERACTIONS:

IMPLICATIONS FOR DIGITAL SOIL MAPPING

LAVRAS – MG

2020

FABIO ARNALDO POMAR AVALOS

TIME SERIES ANALYSIS OF REMOTELY SENSED DATA AS A TOOL FOR VEGETATION EVALUATION AND SOIL-WATER INTERACTIONS:

IMPLICATIONS FOR DIGITAL SOIL MAPPING

Thesis submitted to the Federal University of Lavras, as part of the requirements of the Graduate Program in Soil Science, area of concentration in Environmental Resources and Land Use, to obtain the title of Doctor.

Prof. Dr. Marx Leandro Naves Silva
Advisor

LAVRAS – MG
2020

Ficha catalográfica elaborada pelo Sistema de Geração de Ficha Catalográfica da Biblioteca Universitária da UFLA, com dados informados pelo(a) próprio(a) autor(a).

Avalos, Fabio Arnaldo Pomar.
Time series analysis of remotely sensed data as a tool for vegetation evaluation and soil-water interactions : Implications for digital soil mapping / Fabio Arnaldo Pomar Avalos. - 2020.
74 p. : il.

Orientador(a): Marx Leandro Naves Silva.

Tese (doutorado) - Universidade Federal de Lavras, 2020.
Bibliografia.

1. Índice de vegetação. 2. Umidade do solo. 3. Fenologia de superfície. I. Silva, Marx Leandro Naves. II. Título.

FABIO ARNALDO POMAR AVALOS

TIME SERIES ANALYSIS OF REMOTELY SENSED DATA AS A TOOL FOR VEGETATION EVALUATION AND SOIL-WATER INTERACTIONS:

IMPLICATIONS FOR DIGITAL SOIL MAPPING

Thesis submitted to the Federal University of Lavras, as part of the requirements of the Graduate Program in Soil Science, area of concentration in Environmental Resources and Land Use, to obtain the title of Doctor.

APPROVED on October 29, 2020.

Prof. Dr. Marx Leandro Naves Silva	UFLA
Prof. Dr. Nilton Curi	UFLA
Prof. Dr. Junior Cesar Avanzi	UFLA
Prof. Dr. Fausto Weimar Acerbi Júnior	UFLA
Prof. Dr. Ronaldo Luiz Mincato	UNIFAL

Prof. Dr. Marx Leandro Naves Silva
Advisor

LAVRAS – MG
2020

ACKNOWLEDGEMENTS

I would like to express my gratitude to the Federal University of Lavras (UFLA) and the Soil Science Department (DCS) for the opportunity.

I also recognize my gratitude to the Coordenação de Aperfeiçoamento de Pessoal de Nível Superior – Brasil (CAPES) – Finance Code 001, Programa de Excelência Acadêmica - Proex (AUXPE 593/201), Conselho Nacional de Desenvolvimento Científico e Tecnológico - CNPq (Processos 306511-2017-7 and 202938/2018-2), Fundação de Amparo a Pesquisa do Estado de Minas Gerais - FAPEMIG (Processos APQ-00802-18 and CAG-APQ 01053-15), and Fundação de Amparo à Pesquisa do Estado de São Paulo – FAPESP (ClimateWise 2015/50682-6), CAPES/ANA “Estimativa de evapotranspiração por sensoriamento remoto para gestão de recursos hídricos no Brasil” 88887.144979/2017-00, and CNPq/ANA 446278/2015-7 “O regime hidrológico das bacias dos Rios Piracicaba e Paraíba do Sul no clima futuro: avaliação de alta resolução dos padrões, incertezas e impactos do uso da terra” for their financial support and scholarships.

I deeply thank to my professors: Marx Leandro Naves Silva, Nilton Curi, Junior Cesar Avanzi, Fausto Weimar Acerbi Júnior, Ronaldo Luiz Mincato, Michele Duarte de Menezes, and Marcelo Silva de Oliveira, for their guidance, teachings, and support.

A special thanks to my friends and colleagues in the UFLA's Soil Science Department - my family in Brazil.

Finally, my deepest respect and gratitude to my mother Florencia who always supported me, and all my family.

GENERAL ABSTRACT

Soil, as a synthetic body, is the result of complex environmental interactions occurring across time and different geographic scales. Its functions are critical to maintaining ecosystem services, such as water redistribution and water storage, nutrient cycling, food production, carbon storage and sequestration, and climate regulation. The knowledge of soil geographic distribution and its relation with landscape dynamics are of paramount importance to sustaining such functions. Digital soil mapping (DSM) methods are intended to solve spatial association models that relate geographic occurrence of soil to soil-forming factors, namely: parent material, topography, climate, organisms, and time. Remotely sensed data are essential to parametrize such models, since they offer measurements of land surface features, both in time and geographic frames. However, despite the good performance of the assimilation of data from optical remote sensors with laboratory analysis and field data into DSM, accessing soil properties under vegetation cover via remote sensing methods still represents a challenging task. Therefore, this research intended to evaluate a method to assess the response of vegetation greenness (VG) to soil condition based on the following hypotheses: a) Modulation of surface reflectance of vegetation is controlled by soil condition and properties related to water dynamics, b) this feature can be measured based on remotely sensed data and a time-spectral signature of vegetation response associated to mentioned soil properties can, therefore, be retrieved, c) elucidation of this relationship can be applied to produce time-synthetic covariates for DSM. Although the initial hypothesis was partially verified statistically, VG temporal signal may not reflect exclusively the effects of water availability and other factors can act as vegetation ‘stressors’ affecting its spectral properties, such as the interaction of soil fertility, toxicity, and taxonomic class. Results of this approach demonstrated that the addition of seasonal variability of vegetation greenness can be applied to access soil subsurface processes, as well as their use as covariates in DSM.

Keywords: Vegetation indices. Soil moisture. Land surface phenology. Rainfall seasonality.

RESUMO GERAL

O solo, como um corpo sintético, é o resultado de interações ambientais complexas que ocorrem ao longo do tempo e em diferentes escalas geográficas. Suas funções são críticas para manter serviços ecossistêmicos, como redistribuição e armazenamento de água, ciclagem de nutrientes, produção de alimentos, armazenamento e sequestro de carbono e regulação do clima. O conhecimento da distribuição geográfica do solo e sua relação com a dinâmica da paisagem são de suma importância para sustentar tais funções. Os métodos de mapeamento digital do solo (MDS) visam resolver modelos de associação espacial que relacionam a ocorrência geográfica do solo aos fatores formadores do solo, a saber: material de origem, topografia, clima, organismos e tempo. Os dados de sensoriamento remoto são essenciais para parametrizar tais modelos, uma vez que oferecem medidas das características da superfície da terra, tanto em termos de tempo quanto geográficos. No entanto, apesar do bom desempenho da assimilação de dados de sensores remotos ópticos com dados obtidos em laboratório e dados de campo no MDS, acessar propriedades de solo sob cobertura vegetal por meio de métodos de sensoriamento remoto ainda representa uma tarefa desafiadora. Portanto, esta pesquisa objetivou avaliar um método para analisar a resposta do verdor da vegetação (VG) à condição do solo com base nas seguintes hipóteses: a) A modulação da refletância da superfície da vegetação é controlada pela condição do solo e as propriedades relacionadas à dinâmica da água, b) esta característica pode ser medida com base em dados detectados remotamente e uma assinatura espectro-temporal da resposta da vegetação associada às propriedades do solo mencionadas pode, portanto, ser recuperada, c) a elucidação dessa relação pode ser aplicada para produzir covariáveis sintéticas no tempo para o MDS. Embora a hipótese inicial tenha sido parcialmente verificada estatisticamente, o sinal temporal do VG pode não refletir exclusivamente os efeitos da disponibilidade de água e outros fatores podem atuar como "estressores" da vegetação afetando suas propriedades espectrais, como a interação entre fertilidade do solo, toxicidade e classe taxonômica. Os resultados desta abordagem demonstraram que a adição da variabilidade sazonal do verdor da vegetação pode ser aplicada para acessar os processos de subsuperfície do solo, bem como seu uso como covariáveis no MDS.

Palavras-chave: Índices de vegetação. Umidade do solo. Fenologia de superfície. Sazonalidade da chuva.

SUMMARY

FIRST PART

1 GENERAL INTRODUCTION

Soil, as a synthetic body, is the result of complex environmental interactions occurring across a continuum of geographic and temporal scales. Its functions are critical to maintaining ecosystem services, such as water redistribution and storage, nutrient cycling, food production, carbon storage and sequestration, and climate regulation. The knowledge of soil geographic distribution and its relation with landscape dynamics are of paramount importance for sustaining such functions (BOETTINGER et al., 2010; MCBRATNEY; MENDONÇA SANTOS; MINASNY, 2003; MCBRATNEY; FIELD; KOCH, 2014; RIZZO et al., 2016).

Digital soil mapping (DSM) methods are intended to develop spatial association models that relate geographic occurrence of soil to soil-forming factors, namely: parent material, topography, climate, organisms and vegetation, time, and geographic location (JENNY, 1941; MCBRATNEY; MENDONÇA SANTOS; MINASNY, 2003).

Remotely sensed data (satellite imagery) are essential to parametrize such models since they offer spatially exhaustive measurements of land surface features, both in time and geographic frames (BEN-DOR, 2002; DEMATTÊ; TERRA, 2014; JENSEN, 2007). However, despite the good performance of the assimilation of data from optical remote sensors with laboratory analysis and field data into DSM, accessing soil properties under vegetation cover via remote sensing methods still constitutes a challenging task (ARAÚJO et al., 2014; DEMATTÊ; TERRA, 2014; GENÚ; DEMATTÊ, 2006; MENDES et al., 2019). Additionally, studies that relate remotely sensed vegetation responses (via vegetation indices) to water dynamics at detailed temporal scales are still scarce, remarkably outside temperate regions. Therefore, this research aim to evaluate a method to access subsurface soil under vegetation cover based on the following hypotheses: a) Modulation of surface reflectance of vegetation is controlled by soil condition and properties related to water dynamics, b) this feature can be measured based on remotely sensed data and a time-spectral signature of vegetation response associated to mentioned soil properties can, therefore, be retrieved, c) elucidation of this relationship can be applied to produce time-synthetic covariates for digital soil mapping.

2 THEORETICAL BACKGROUND

2.1 Remote sensing of soil and vegetation

Optical remote sensing (RS) is a measurement technique applied to collect data on the interaction between electromagnetic radiation (EMR) emitted from a natural source (i.e. the Sun) and land surface. Data recorded remotely is available in the format of a grid of cells, which is termed as 'raster'. Raster data format has the following properties: location, spatial resolution, and digital number (JENSEN, 2007; SCULL et al., 2003). In addition to the mentioned properties, EMR data obtained by RS is also characterized by its spectral, radiometric, and temporal resolutions (JENSEN, 2007). Remote sensing data resolutions and associated metrics (e.g. signal-to-noise ratio) are crucial for the accuracy and reliability of RS products (TEILLET; STAENZ; WILLIAMS, 1997).

The increasing availability of RS data has resulted in important developments in the study of land surface processes, being among the most used sensors: Thematic Mapper (TM), Enhanced Thematic Mapper (ETM+), Operational Land Imager and Thermal Infrared Sensor (OLI/TIRS) carried by the Landsat satellites (DWYER et al., 2018), Moderate Resolution Imaging Spectroradiometer (MODIS), which is aboard the Terra and Aqua satellites (PAGANO; DURHAM, 1993), and MultiSpectral Instrument (MSI) of the Sentinel 2 satellites (PAHLEVAN et al., 2017).

Table 1 – Resolutions of the most used optical remote sensors.

Satellite - Sensor	**Resolution**		
	Spatial	**Radiometric**	**Temporal**
Landsat 5 - Thematic Mapper	15, 30, 120 m	8 bits	16 days
Landsat 8 - Operational Land Imager	15, 30, 60 m	12 bits	16 days
Sentinel 2 - Multi Spectral Imager	10, 20, 60 m	12 bits	5 days
Terra & Aqua - Moderate Resolution Imaging Spectroradiometer	250 m - 1 km	12 bits	1, 2 days

Source: Adapted from Jensen (2007)

Remote analysis of land processes related to soil properties is supported, for the most part, by the interaction between electromagnetic radiation and the constituent elements of soil, which are referred to as chromophores. Soil chromophores can be classified into minerals (clay,

iron oxides, soluble salts), organic matter (fresh or decomposed), and water (BEN-DOR, 2002). Due to that relationship, it is verified that the data obtained by optical remote sensing (RS) in the spectral region of 400 to 2500 nm displays characteristic responses to different soil types and attributes in specific regions of the electromagnetic spectrum (ALEXANDRE et al., 2010; BEN-DOR, 2002; BEN-DOR et al., 2008; DEMATTÊ et al., 2015), constituting what is called as 'spectral signature' (Figure 1). Underpinned by that fact, an important quantity of research has reported the possibility of inferring soil properties such as granulometric composition, water content, electromagnetic properties, organic matter, and presence of minerals in the clay fraction (ALVES; DEMATTÊ; BARROS, 2015; BEN-DOR et al., 2009; DEMATTÊ; TERRA, 2014; DEMATTÊ et al., 2016a; GENÚ; DEMATTÊ, 2006; MULDER et al., 2011; RIZZO et al., 2016).

Vegetation interaction with EMR is driven by green leaf constituents: photosynthetic pigments, water, and intercellular air spaces (JENSEN, 2007), having its spectral signal conditioned by their variations, which are responses to genetic constitution and environmental conditions (Figure 2).

Figure 1 – Spectrum representing the major soil chromophores.

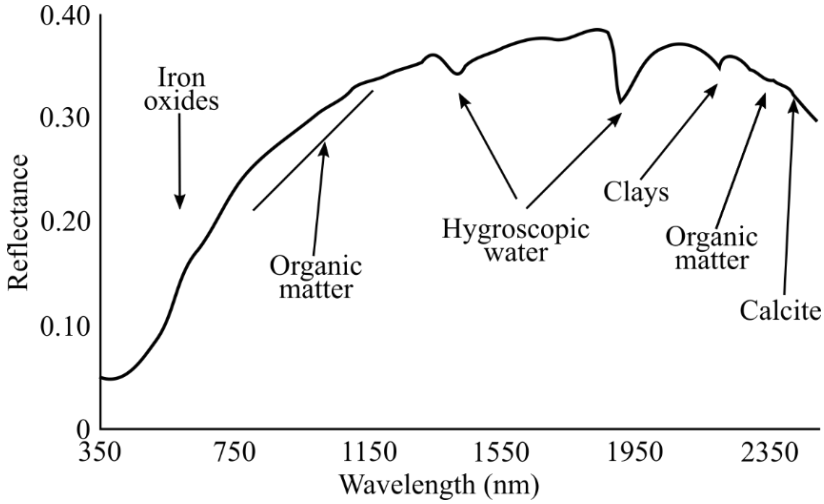

Source: Adapted from Ben-Dor *et al.* (2008)

Remote sensing of vegetation has been used extensively to assess the state of different types of vegetation and soil covers. Remarkably through vegetation indices (VIs), for instance, the normalized difference vegetation index (NDVI, HUETE; JACKSON, 1987) and enhanced vegetation index (EVI, HUETE et al., 2002). NDVI is based on the relationship between red (640 - 670 nm) and near-infrared (850 - 880 nm) spectral bands (Equation 1), which have been

reported of great importance for the study of vegetation; being that chlorophyll is absorbed in the visible region (red band) and that the effects of plant structure are observable in the near-infrared band (JENSEN, 2007). Similarly to NDVI, EVI (Equation 2) also makes use of the red-near-infrared relationship, but it adds information of the blue band (450-510 nm); by doing this, the EVI intends to maintain sensitivity over dense vegetation regions as well as the attenuation of some atmospheric effects (HUETE et al., 2002). On account of its simplicity and early availability, NDVI is the most used proxy of vegetation greenness.

$$NDVI = \frac{\rho_{NIR} - \rho_R}{\rho_{NIR} + \rho_R} \tag{1}$$

$$EVI = G \times \frac{\rho_{NIR} - \rho_R}{\rho_{NIR} + C_1\rho_R - C_2\rho_B + L} \tag{2}$$

Where: ρ are surface reflectances for its corresponding spectral bands (*NIR*: near-infrared, *R*: red, *B*: blue), *G* is a gain factor, *L* is an adjustment factor related to canopy effects, and C_1 and C_2 are the coefficients for aerosol resistance. Ideally, vegetation indices are calculated from atmospherically-corrected surface reflectance.

Figure 2 – Typical spectral signature of green vegetation.

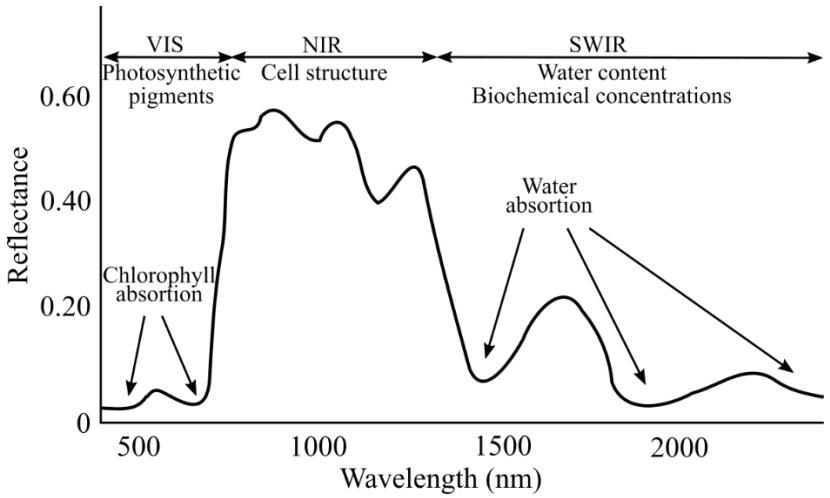

VIS: Visible, NIR: near infrared, SWIR: small-wave infrared.
Source: Adapted from Gholizadeh and Kopačková (2019).

Regarding the relation between temporal variability of VIs and soil-water dynamics, Santos et al. (2014) observed strong lagged correlations between soil water content and spectral vegetation-response at management scale, as a function of rainfall, soil depth, and water

absorption in the root-zone. Also strong lagged correlations between soil water content and greenness-based indices, i.e. NDVI, are reported by Liu et al. (2012); who discussed the evidence of phenology-seasonal relations in a water-limited environment. Furthermore, the same study remarked the necessity of additional soil properties and topography to refine the analysis. Ahmed et al. (2017) also demonstrated that time-series of satellite imagery can be used to analyze soil-vegetation interactions at broad scales. The mentioned studies used coarse spatial resolutions (between 250 and 1000 m).

At broader scales (> 1000 m), evidence of soil control on vegetation productivity assessed by the NDVI has been verified by Nicholson and Farrar (1994) and Farrar, Nicholson and Lare (1994). These authors analyzed the interaction among rainfall, soil type, soil moisture, and NDVI, and found that Vertisols are associated with higher vegetation productivities, evaluated as the ratio of NDVI to rainfall, in contrast to Arenosols and Solonchaks.

2.2 Time-series of vegetation indices

Availability of time-series of remotely sensed data has enabled the analysis of temporal variability of vegetation indices and its association with the life-cycles of plants, i.e. phenological patterns. When such analysis is based on optical remote sensing data it is termed as land surface phenology - LSP (HELMAN, 2018).

Figure 3 – Array of vegetation index data for the extraction of time-series.

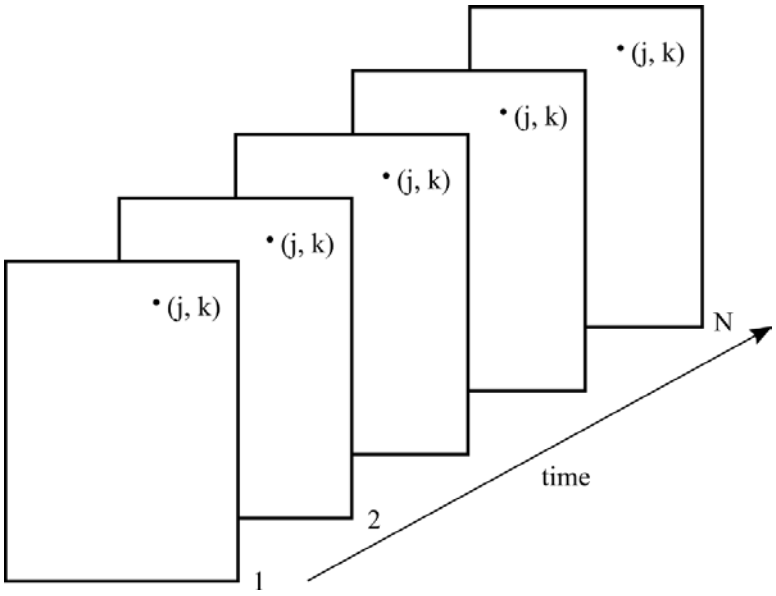

Source: Jönsson and Eklundh (2004)

To extract information related to the temporal variability of a VI, time-series are constructed following the scheme in Figure 3, where (j, k) is the spatial position for a particular VI measurement, that is extracted consecutive times (i = 1, 2, ..., N) from an image I, constituting a time-series (t_i, I_i).

LSP metrics aim to measure and synthesize the seasonal variation of vegetation when assessed by a vegetation index (e.g. NDVI or EVI). Decadal databases of satellite imagery are currently available from websites such as Application for Extracting and Exploring Analysis Ready Samples (AρρEEARS) at https://lpdaacsvc.cr.usgs.gov/appeears/ or Google Earth Engine (earth.egnine.com). The Landsat program, for example, offers nearly 40 years of observations, and as the result of cloud-based computation tools, preprocessing steps that used to consume high computational resources, such as co-registration, geometric, radiometric, and atmospheric corrections, have led to the availability of 'analysis-ready data', which is critical for analyses that include the temporal dimension (WULDER et al., 2012).

Monitoring NDVI or EVI in a temporal frame can reveal seasonal changes, natural or human-driven, in vegetation. Studies exploiting this feature showed important developments in the study of land surface phenology, drought monitoring, ecosystemic disturbances, and deforestation (COHEN; YANG; KENNEDY, 2010; CUNHA et al., 2015; HELMAN, 2018; LIU et al., 2017; VERBESSELT et al., 2010a, 2010b; VERBESSELT; ZEILEIS; HEROLD, 2012).

Figure 4 – Phenological metrics produced by the TIMESAT algorithm.

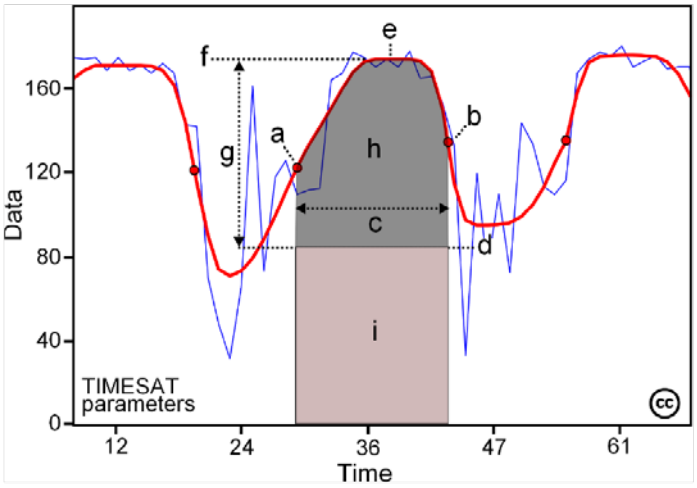

Where: a: beginning of season, b: end of season, c: length of season, d: base value, e: time of middle of season, f: maximum value, g: amplitude, h: small integrated value, h + i: large integrated value.

Source: Eklundh and Jönsson (2017).

2.3 Digital soil mapping

Knowledge of the geographic distribution of soil at detailed scales is a global concern, especially in the current scenario of human-driven environmental threats related to the sustainability of soil ecosystem services, such as water scarcity, soil carbon emission to the atmosphere, and accelerated soil degradation and erosion (GUO et al., 2019; MCBRATNEY; FIELD; KOCH, 2014; MONTANARELLA et al., 2016).

Digital soil mapping (DSM) techniques are underpinned by a well-known and widely accepted model in soil science: the factors of soil formation; which serve as a link between soil formation processes and five recognized drivers: climate (c), organisms and vegetation (o), relief (r), parent material (p) and time (t). Early efforts to bring a quantitative solution to the factor model can be traced back to the work of Jenny (1941). Currently, as a result of the development of geographic information technology and data science, a comprehensive digital framework can be applied for the production of digital soil maps (BREVIK et al., 2016; MCBRATNEY; MENDONÇA SANTOS; MINASNY, 2003; MILLER; SCHAETZL, 2014). Currently, the scorpan model, as formalized by McBratney *et al.* (2003), serves as a pipeline for the production of digital soil maps.

The mentioned approach has shown good performances when integrating remotely sensed data into DSM. Outstandingly, the use of digital elevation models (DEM) and its derived terrain attributes, The most used DEM data was retrieved based on radar interferometry from the shuttle radar topography mission - SRTM (FARR et al., 2007). SRTM DEMs have been included into the DSM production line successfully, as is observed in different studies (BISHOP; MINASNY; MCBRATNEY, 2006; HENGL et al., 2017; HENGL; HEUVELINK; ROSSITER, 2007; MOURA-BUENO et al., 2016; PADARIAN; MINASNY; MCBRATNEY, 2015; TENG et al., 2016), where DEM and terrain attributes are interpreted as the relief factor (r).

Optical remote sensing (RS) data have also been integrated into the DSM methodology (HENGL et al., 2017b; MCBRATNEY; MENDONÇA SANTOS; MINASNY, 2003), where it has followed two approaches. The first one is when RS and VIs data are interpreted as a proxy for the organisms and vegetation factor (o), as is the case in Chagas *et al.* (2016), Padarian *et al.* (2015), Silva *et al.* (2019), and Taghizadeh-Mehrjardi *et al.* (2015). The second approach is when remotely sensed imagery is compared quantitatively to the reflectance of soil samples measured in the laboratory and associated with its corresponding geographic locations. The

advantage of this approach over the first one is that allows physical interpretations, enabling the possibility to infer other soil properties (ALEXANDRE et al., 2010; DEMATTÊ; TERRA, 2014; DEMATTÊ et al., 2016b, 2016a; NANNI et al., 2011; NANNI; DEMATTÊ, 2006; RAMIREZ-LOPEZ et al., 2013a, 2013b; VASQUES et al., 2014). Such an approach became of such importance that local and global efforts are being carried out into developing soil spectral libraries (ARAÚJO *et al.*, 2014; BELLINASO; DEMATTÊ; ROMEIRO, 2010; TERRA; DEMATTÊ; VISCARRA ROSSEL, 2015; VISCARRA ROSSEL *et al.*, 2016).

Recently, analysis of the temporal variability of VIs has been assessed specifically for DSM applications (DEMATTÊ et al., 2017; MAYNARD; LEVI, 2017). The dimension of the temporal databases analyzed ranged from bi-temporal (two images) to hyper-temporal approaches (> 100 images).

3 FINAL REMARKS

Optical remote sensing has become an essential tool for analyzing land surface processes, notably when combined with temporal criteria. Despite showing good performances when assimilated into DSM, soil remote sensing still have as the main constraint to its application to the occurrence of soils under permanent vegetation cover, which hampers direct comparisons with reflectance obtained in the laboratory. Such a fact calls for the development of techniques that can extract information suitable for the production of digital soil maps in inaccessible areas by the current methods. Since soil and water interactions support directly the development of plants by affecting its spectral properties, its monitoring and analysis by remote methods can reveal subsurface soil conditions, especially those related to water content and nutrient availability. By doing this, it can be possible to elucidate time-response signatures of vegetation to soil conditions and bringing out new insights about soil subsurface processes and the plant-soil system.

REFERENCES

AHMED, Mohamed; ELSE, Brent; EKLUNDH, Lars; ARDÖ, Jonas; SEAQUIST, Jonathan. Dynamic response of NDVI to soil moisture variations during different hydrological regimes in the Sahel region. **International Journal of Remote Sensing**, v. 38, n. 19, p. 5408–5429, 2017. DOI: 10.1080/01431161.2017.1339920. Available at: https://doi.org/10.1080/01431161.2017.1339920.

ALEXANDRE, José; DEMATTÊ, Melo; DA, Fabrício; TERRA, Silva. Comportamento espectral de perfis modais dos principais solos de rafard , SP. **Bragantia**, v. 69, n. 2, p. 249–252, 2010.

ALVES, Marcelo Rodrigo; DEMATTÊ, José A. M.; BARROS, Pedro Paulo Silva. Multiple Geotechnological Tools Applied to Digital Mapping of Tropical Soils. **Revista Brasileira de Ciência do Solo**, v. 39, n. 5, p. 1261–1274, 2015. DOI: 10.1590/01000683rbcs20140410. Available at: http://www.scielo.br/scielo.php?script=sci_arttext&pid=S0100-06832015000501261&lng=en&nrm=iso&tlng=en.

ARAÚJO, S. R.; WETTERLIND, J.; DEMATTÊ, J. A. M.; STENBERG, B. Improving the prediction performance of a large tropical vis-NIR spectroscopic soil library from Brazil by clustering into smaller subsets or use of data mining calibration techniques. **European Journal of Soil Science**, v. 65, n. 5, p. 718–729, 2014. DOI: 10.1111/ejss.12165. Available at: http://doi.wiley.com/10.1111/ejss.12165.

BELLINASO, Henrique; DEMATTÊ, José Alexandre Melo; ROMEIRO, Suzana Araújo. Soil spectral library and its use in soil classification. **Revista Brasileira de Ciência do Solo**, v. 34, n. 3, p. 861–870, 2010. DOI: 10.1590/S0100-06832010000300027. Available at: http://www.scielo.br/scielo.php?script=sci_arttext&pid=S0100-06832010000300027&lng=en&tlng=en.

BEN-DOR, E. Quantitative remote sensing of soil properties. **Advances in Agronomy**, v. 75, p. 173–243, 2002.

BEN-DOR, E.; CHABRILLAT, S.; DEMATTÊ, J. A. M.; TAYLOR, G. R.; HILL, J.; WHITING, M. L.; SOMMER, S. Using Imaging Spectroscopy to study soil properties. **Remote Sensing of Environment**, v. 113, n. SUPPL. 1, p. S38–S55, 2009. DOI: 10.1016/j.rse.2008.09.019. Available at: http://dx.doi.org/10.1016/j.rse.2008.09.019.

BEN-DOR, E.; TAYLOR, R. G.; HILL, J.; DEMATTÊ, J. A. M.; WHITING, M. L.; CHABRILLAT, S.; SOMMER, S. Imaging Spectrometry for Soil Applications. *In*: **Advances in Agronomy**. v. 97p. 321–392. DOI: 10.1016/S0065-2113(07)00008-9. Available at: https://linkinghub.elsevier.com/retrieve/pii/S0065211307000089.

BISHOP, T. F. A.; MINASNY, B.; MCBRATNEY, A. B. Uncertainty analysis for soil-terrain models. **International Journal of Geographical Information Science**, v. 20, n. 2, p. 117–134, 2006. DOI: 10.1080/13658810500287073. Available at: http://www.tandfonline.com/doi/abs/10.1080/13658810500287073.

BOETTINGER, J. L.; HOWELL, D. W.; MOORE, A. C.; HARTEMINK, A. E.; KIENAST-BROWN, S. **Digital Soil Mapping, Bridging Research, Environmental Application and Operation**: Springer, 2010.

BREVIK, Eric C.; CALZOLARI, Costanza; MILLER, Bradley A.; PEREIRA, Paulo;

KABALA, Cezary; BAUMGARTEN, Andreas; JORDÁN, Antonio. Soil mapping, classification, and pedologic modeling: History and future directions. **Geoderma**, v. 264, p. 256–274, 2016. DOI: 10.1016/j.geoderma.2015.05.017. Available at: https://linkinghub.elsevier.com/retrieve/pii/S0016706115001718.

CHAGAS, César da Silva; DE CARVALHO JUNIOR, Waldir; BHERING, Silvio Barge; CALDERANO FILHO, Braz. Spatial prediction of soil surface texture in a semiarid region using random forest and multiple linear regressions. **CATENA**, v. 139, p. 232–240, 2016. DOI: 10.1016/j.catena.2016.01.001. Available at: http://dx.doi.org/10.1016/j.catena.2016.01.001.

COHEN, Warren B.; YANG, Zhiqiang; KENNEDY, Robert. Detecting trends in forest disturbance and recovery using yearly Landsat time series: 2. TimeSync — Tools for calibration and validation. **Remote Sensing of Environment**, v. 114, n. 12, p. 2911–2924, 2010. DOI: 10.1016/j.rse.2010.07.010. Available at: http://dx.doi.org/10.1016/j.rse.2010.07.010.

CUNHA, A. P. M.; ALVALÁ, R. C.; NOBRE, C. A.; CARVALHO, M. A. Monitoring vegetative drought dynamics in the Brazilian semiarid region. **Agricultural and Forest Meteorology**, v. 214–215, n. June 2018, p. 494–505, 2015. DOI: 10.1016/j.agrformet.2015.09.010. Available at: http://dx.doi.org/10.1016/j.agrformet.2015.09.010.

DEMATTÊ, J. A. M.; TERRA, F. S. Spectral pedology: A new perspective on evaluation of soils along pedogenetic alterations. **Geoderma**, v. 217–218, p. 190–200, 2014.

DEMATTÊ, José A. M.; ARAÚJO, Suzana Romero; FIORIO, Peterson Ricardo; FONGARO, Caio Troula; NANNI, Marcos Rafael. VIS-NIR-SWIR spectroscopy in soil evaluation along a toposequence in Piracicaba. **REVISTA CIÊNCIA AGRONÔMICA**, v. 46, n. 4, p. 679–688, 2015. DOI: 10.5935/1806-6690.20150054. Available at: http://www.gnresearch.org/doi/10.5935/1806-6690.20150054.

DEMATTÊ, José A. M.; SAYÃO, Veridiana Maria; RIZZO, Rodnei; FONGARO, Caio T. Soil class and attribute dynamics and their relationship with natural vegetation based on satellite remote sensing. **Geoderma**, v. 302, n. March 2016, p. 39–51, 2017. DOI: 10.1016/j.geoderma.2017.04.019. Available at: http://dx.doi.org/10.1016/j.geoderma.2017.04.019.

DEMATTÊ, José Alexandre Melo; ALVES, Marcelo Rodrigo; TERRA, Fabricio da Silva; BOSQUILIA, Raoni Wainer Duarte; FONGARO, Caio Troula; BARROS, Pedro Paulo da Silva. Is It Possible to Classify Topsoil Texture Using a Sensor Located 800 km Away from the Surface? **Revista Brasileira de Ciência do Solo**, v. 40, p. 1–13, 2016. a. DOI: 10.1590/18069657rbcs20150335. Available at: http://www.scielo.br/scielo.php?script=sci_arttext&pid=S0100-06832016000100311&lng=en&tlng=en.

DEMATTÊ, José; RAMIREZ-LOPEZ, Leonardo; RIZZO, Rodnei; NANNI, Marcos; FIORIO, Peterson; FONGARO, Caio; MEDEIROS NETO, Luiz; SAFANELLI, José; DA S. BARROS, Pedro. Remote Sensing from Ground to Space Platforms Associated with Terrain Attributes as a Hybrid Strategy on the Development of a Pedological Map. **Remote Sensing**, v. 8, n. 10, p. 826, 2016. b. DOI: 10.3390/rs8100826. Available at: http://www.mdpi.com/2072-4292/8/10/826.

DWYER, John L.; ROY, David P.; SAUER, Brian; JENKERSON, Calli B.; ZHANG, Hankui K.; LYMBURNER, Leo. Analysis ready data: Enabling analysis of the landsat archive. **Remote Sensing**, v. 10, n. 9, p. 1–19, 2018. DOI: 10.3390/rs10091363.

EKLUNDH, L.; JÖNSSON, P. **Timesat - Software Manual**SwedenLund and Malmö University, 2017. Available at: http://www.nateko.lu.se/TIMESAT/.

FARR, T. et al. The shuttle radar topography mission. **Reviews of Geophysics**, v. 45, p. 1–33, 2007. DOI: 10.1029/2005RG000183.1.INTRODUCTION.

FARRAR, T.; NICHOLSON, S.; LARE, A. The influence of soil type on the relationships between NDVI, rainfall, and soil moisture in semiarid Botswana. II. NDVI response to soil moisture. **Remote Sensing of Environment**, v. 50, n. 2, p. 121–133, 1994. DOI: 10.1016/0034-4257(94)90039-6. Available at: https://linkinghub.elsevier.com/retrieve/pii/0034425794900396.

GENÚ, A. M.; DEMATTÊ, J. A. M. Determination of soil attribute contents by means of reflected electromagnetic energy. **International Journal of Remote Sensing**, v. 27, n. 21, p. 4807–4818, 2006. DOI: 10.1080/01431160600568926. Available at: http://www.tandfonline.com/doi/abs/10.1080/01431160600568926.

GHOLIZADEH, A.; KOPAČKOVÁ, V. Detecting vegetation stress as a soil contamination proxy: a review of optical proximal and remote sensing techniques. **International Journal of Environmental Science and Technology**, v. 16, n. 5, p. 2511–2524, 2019. DOI: 10.1007/s13762-019-02310-w. Available at: http://link.springer.com/10.1007/s13762-019-02310-w.

GUO, Yanrong; PENG, Changhui; ZHU, Qiuan; WANG, Meng; WANG, Han; PENG, Shushi; HE, Honglin. Modelling the impacts of climate and land use changes on soil water erosion: Model applications, limitations and future challenges. **Journal of Environmental Management**, v. 250, n. July, p. 109403, 2019. DOI: 10.1016/j.jenvman.2019.109403. Available at: https://doi.org/10.1016/j.jenvman.2019.109403.

HELMAN, David. Land surface phenology: What do we really 'see' from space? **Science of The Total Environment**, v. 618, p. 665–673, 2018. DOI: 10.1016/j.scitotenv.2017.07.237. Available at: https://doi.org/10.1016/j.scitotenv.2017.07.237.

HENGL, Tomislav et al. SoilGrids250m: Global gridded soil information based on machine learning. **PLOS ONE**, v. 12, n. 2, p. e0169748, 2017. a. DOI: 10.1371/journal.pone.0169748. Available at: http://dx.plos.org/10.1371/journal.pone.0169748.

HENGL, Tomislav et al. Soil nutrient maps of Sub-Saharan Africa: assessment of soil nutrient content at 250 m spatial resolution using machine learning. **Nutrient Cycling in Agroecosystems**, v. 109, n. 1, p. 77–102, 2017. b. DOI: 10.1007/s10705-017-9870-x. Available at: http://link.springer.com/10.1007/s10705-017-9870-x.

HENGL, Tomislav; HEUVELINK, Gerard B. M.; ROSSITER, David G. About regression-kriging: From equations to case studies. **Computers & Geosciences**, v. 33, n. 10, p. 1301–1315, 2007. DOI: 10.1016/j.cageo.2007.05.001. Available at: http://linkinghub.elsevier.com/retrieve/pii/S0098300407001008. Acesso em: 27 maio. 2014.

HUETE, A.; DIDAN, K.; MIURA, T.; RODRIGUEZ, E. P.; GAO, X.; FERREIRA, L. G. Overview of the radiometric and biophysical performance of the MODIS vegetation indices.

Remote Sensing of Environment, v. 83, p. 195–213, 2002. DOI: 10.1080/0965156X.2013.836857. Available at: https://www.tandfonline.com/doi/full/10.1080/0965156X.2013.836857.

JENNY, H. **Factors of Soil Formation, A System of Quantitative Pedology**. New York: McGraw-Hill, 1941.

JENSEN, J. R. **Remote sensing of the environment: an earth resource perspective**: Pearson Prentice Hall, 2007.

JÖNSSON, Per; EKLUNDH, Lars. TIMESAT—a program for analyzing time-series of satellite sensor data. **Computers & Geosciences**, v. 30, n. 8, p. 833–845, 2004. DOI: 10.1016/j.cageo.2004.05.006. Available at: https://linkinghub.elsevier.com/retrieve/pii/S0098300404000974.

LIU, Shishi; ROBERTS, Dar A.; CHADWICK, Oliver A.; STILL, Chris J. Spectral responses to plant available soil moisture in a Californian grassland. **International Journal of Applied Earth Observation and Geoinformation**, v. 19, n. 1, p. 31–44, 2012. DOI: 10.1016/j.jag.2012.04.008. Available at: http://dx.doi.org/10.1016/j.jag.2012.04.008.

LIU, Yan et al. Using data from Landsat, MODIS, VIIRS and PhenoCams to monitor the phenology of California oak/grass savanna and open grassland across spatial scales. **Agricultural and Forest Meteorology**, v. 237–238, p. 311–325, 2017. DOI: 10.1016/j.agrformet.2017.02.026. Available at: http://dx.doi.org/10.1016/j.agrformet.2017.02.026.

MAYNARD, Jonathan J.; LEVI, Matthew R. Hyper-temporal remote sensing for digital soil mapping: Characterizing soil-vegetation response to climatic variability. **Geoderma**, v. 285, p. 94–109, 2017. DOI: 10.1016/j.geoderma.2016.09.024. Available at: http://dx.doi.org/10.1016/j.geoderma.2016.09.024.

MCBRATNEY, AB A. ..; MENDONÇA SANTOS, M. ..; MINASNY, B. On digital soil mapping. **Geoderma**, v. 117, n. 1–2, p. 3–52, 2003. DOI: 10.1016/S0016-7061(03)00223-4. Available at: http://linkinghub.elsevier.com/retrieve/pii/S0016706103002234. Acesso em: 5 out. 2017.

MCBRATNEY, Alex; FIELD, Damien J.; KOCH, Andrea. The dimensions of soil security. **Geoderma**, v. 213, p. 203–213, 2014. DOI: 10.1016/j.geoderma.2013.08.013. Available at: http://dx.doi.org/10.1016/j.geoderma.2013.08.013.

MENDES, Wanderson de S.; MEDEIROS NETO, Luiz G.; DEMATTÊ, José A. M.; GALLO, Bruna C.; RIZZO, Rodnei; SAFANELLI, José L.; FONGARO, Caio T. Is it possible to map subsurface soil attributes by satellite spectral transfer models? **Geoderma**, v. 343, n. February, p. 269–279, 2019. DOI: 10.1016/j.geoderma.2019.01.025. Available at: https://doi.org/10.1016/j.geoderma.2019.01.025.

MILLER, B. A.; SCHAETZL, R. J. The historical role of base maps in soil geography. **Geoderma**, v. 230–231, p. 329–339, 2014. DOI: 10.1016/j.geoderma.2014.04.020.

MONTANARELLA, Luca et al. World's soils are under threat. **SOIL**, v. 2, n. 1, p. 79–82, 2016. DOI: 10.5194/soil-2-79-2016. Available at: https://www.soil-journal.net/2/79/2016/.

MOURA-BUENO, Jean Michel; DALMOLIN, Ricardo Simão Diniz; TEN CATEN, Alexandre; RUIZ, Luis Fernando Chimelo; RAMOS, Priscila Vogelei; DOTTO, André

Carnieletto. Assessment of Digital Elevation Model for Digital Soil Mapping in a Watershed with Gently Undulating Topography. **Revista Brasileira de Ciência do Solo**, v. 40, p. 1–15, 2016. DOI: 10.1590/18069657rbcs20150022. Available at: http://www.scielo.br/scielo.php?script=sci_arttext&pid=S0100-06832016000100304&lng=en&nrm=iso&tlng=en.

MULDER, V. L.; DE BRUIN, S.; SCHAEPMAN, M. E.; MAYR, T. R. The use of remote sensing in soil and terrain mapping — A review. **Geoderma**, v. 162, n. 1–2, p. 1–19, 2011. DOI: 10.1016/j.geoderma.2010.12.018. Available at: http://www.sciencedirect.com/science/article/pii/S0016706110003976. Acesso em: 12 jul. 2014.

NANNI, Marcos Rafael; ALEXANDRE, José; DEMATTÊ, Melo; CHICATI, Marcelo Luiz; DE, Roney Berti; CÉZAR, Everson. Spectroradiometric data as support to soil classification. **Journal of Agricultural Science and Soil Science**, v. 1, n. 4, p. 109–117, 2011.

NANNI, Marcos Rafael; DEMATTÊ, José Alexandre M. Spectral Reflectance Methodology in Comparison to Traditional Soil Analysis. **Soil Science Society of America Journal**, v. 70, n. 2, p. 393, 2006. DOI: 10.2136/sssaj2003.0285. Available at: https://www.soils.org/publications/sssaj/abstracts/70/2/393.

NICHOLSON, S.; FARRAR, T. The influence of soil type on the relationships between NDVI, rainfall, and soil moisture in semiarid Botswana. I. NDVI response to rainfall. **Remote Sensing of Environment**, v. 50, n. 2, p. 107–120, 1994. DOI: 10.1016/0034-4257(94)90038-8. Available at: https://linkinghub.elsevier.com/retrieve/pii/0034425794900388.

PADARIAN, J.; MINASNY, B.; MCBRATNEY, A. B. Using Google's cloud-based platform for digital soil mapping. **Computers & Geosciences**, v. 83, p. 80–88, 2015. DOI: 10.1016/j.cageo.2015.06.023. Available at: http://dx.doi.org/10.1016/j.cageo.2015.06.023.

PAGANO, Thomas S.; DURHAM, Rodney M. Moderate Resolution Imaging Spectroradiometer (MODIS). *In*: OPTICAL ENGINEERING AND PHOTONICS IN AEROSPACE SENSING 1993, **Anais** [...]. p. 2–17. DOI: 10.1117/12.152835.

PAHLEVAN, N.; SARKAR, S.; FRANZ, B. A.; BALASUBRAMANIAN, S. V.; HE, J. Sentinel-2 MultiSpectral Instrument (MSI) data processing for aquatic science applications: Demonstrations and validations. **Remote Sensing of Environment**, v. 201, n. May, p. 47–56, 2017. DOI: 10.1016/j.rse.2017.08.033. Available at: https://linkinghub.elsevier.com/retrieve/pii/S0034425717303991.

RAMIREZ-LOPEZ, L.; BEHRENS, T.; SCHMIDT, K.; ROSSEL, R. A. Viscarra; DEMATTÊ, J. A. M.; SCHOLTEN, T. Distance and similarity-search metrics for use with soil vis–NIR spectra. **Geoderma**, v. 199, p. 43–53, 2013. a. DOI: 10.1016/j.geoderma.2012.08.035. Available at: http://dx.doi.org/10.1016/j.geoderma.2012.08.035.

RAMIREZ-LOPEZ, Leonardo; BEHRENS, Thorsten; SCHMIDT, Karsten; STEVENS, Antoine; DEMATTÊ, Jose Alexandre M.; SCHOLTEN, Thomas. The spectrum-based learner: A new local approach for modeling soil vis–NIR spectra of complex datasets. **Geoderma**, v. 195–196, p. 268–279, 2013. b. DOI: 10.1016/j.geoderma.2012.12.014. Available at: http://dx.doi.org/10.1016/j.geoderma.2012.12.014.

RIZZO, Rodnei; DEMATTÊ, José A. M.; LEPSCH, Igo F.; GALLO, Bruna C.; FONGARO,

Caio T. Digital soil mapping at local scale using a multi-depth Vis–NIR spectral library and terrain attributes. **Geoderma**, v. 274, p. 18–27, 2016. DOI: 10.1016/j.geoderma.2016.03.019. Available at: http://dx.doi.org/10.1016/j.geoderma.2016.03.019.

SANTOS, Walbert Júnior Reis; SILVA, Bruno Montoani; OLIVEIRA, Geraldo César; VOLPATO, Margarete Marin Lordelo; LIMA, José Maria; CURI, Nilton; MARQUES, João José. Soil moisture in the root zone and its relation to plant vigor assessed by remote sensing at management scale. **Geoderma**, v. 221–222, p. 91–95, 2014. DOI: 10.1016/j.geoderma.2014.01.006. Available at: http://linkinghub.elsevier.com/retrieve/pii/S0016706114000159.

SCULL, P.; FRANKLIN, J.; CHADWICK, O. A.; MCARTHUR, D. Predictive soil mapping: a review. **Progress in physical geography**, v. 27, n. 2, p. 171–197, 2003.

SILVA, Bárbara Pereira Christofaro; SILVA, Marx Leandro Naves; AVALOS, Fabio Arnaldo Pomar; DE MENEZES, Michele Duarte; CURI, Nilton. Digital soil mapping including additional point sampling in Posses ecosystem services pilot watershed, southeastern Brazil. **Scientific Reports**, v. 9, n. 1, p. 13763, 2019. DOI: 10.1038/s41598-019-50376-w. Available at: http://www.nature.com/articles/s41598-019-50376-w.

TAGHIZADEH-MEHRJARDI, R.; NABIOLLAHI, K.; MINASNY, B.; TRIANTAFILIS, J. Comparing data mining classifiers to predict spatial distribution of USDA-family soil groups in Baneh region, Iran. **Geoderma**, v. 253–254, p. 67–77, 2015. DOI: 10.1016/j.geoderma.2015.04.008. Available at: http://linkinghub.elsevier.com/retrieve/pii/S0016706115001147.

TEILLET, P.; STAENZ, K.; WILLIAMS, DJ. Effects of spectral, spatial, and radiometric characteristics on remote sensing vegetation indices of forested regions. **Remote Sensing of Environment**, v. 61, n. 1, p. 139–149, 1997. DOI: 10.1016/S0034-4257(96)00248-9. Available at: https://linkinghub.elsevier.com/retrieve/pii/S0034425796002489.

TENG, Hongfen; VISCARRA ROSSEL, Raphael A.; SHI, Zhou; BEHRENS, Thorsten; CHAPPELL, Adrian; BUI, Elisabeth. Assimilating satellite imagery and visible–near infrared spectroscopy to model and map soil loss by water erosion in Australia. **Environmental Modelling & Software**, v. 77, p. 156–167, 2016. DOI: 10.1016/j.envsoft.2015.11.024. Available at: http://dx.doi.org/10.1016/j.envsoft.2015.11.024.

TERRA, Fabrício S.; DEMATTÊ, José A. M.; VISCARRA ROSSEL, Raphael A. Spectral libraries for quantitative analyses of tropical Brazilian soils: Comparing vis–NIR and mid-IR reflectance data. **Geoderma**, v. 255–256, p. 81–93, 2015. DOI: 10.1016/j.geoderma.2015.04.017. Available at: http://dx.doi.org/10.1016/j.geoderma.2015.04.017.

VASQUES, G. M.; DEMATTÊ, J. A. M.; VISCARRA ROSSEL, Raphael A.; RAMÍREZ-LÓPEZ, L.; TERRA, F. S. Soil classification using visible/near-infrared diffuse reflectance spectra from multiple depths. **Geoderma**, v. 223–225, n. 1, p. 73–78, 2014. DOI: 10.1016/j.geoderma.2014.01.019. Available at: http://dx.doi.org/10.1016/j.geoderma.2014.01.019.

VERBESSELT, Jan; HYNDMAN, Rob; NEWNHAM, Glenn; CULVENOR, Darius. Detecting trend and seasonal changes in satellite image time series. **Remote Sensing of Environment**, v. 114, n. 1, p. 106–115, 2010. a. DOI: 10.1016/j.rse.2009.08.014. Available at: http://dx.doi.org/10.1016/j.rse.2009.08.014.

VERBESSELT, Jan; HYNDMAN, Rob; ZEILEIS, Achim; CULVENOR, Darius. Phenological change detection while accounting for abrupt and gradual trends in satellite image time series. **Remote Sensing of Environment**, v. 114, n. 12, p. 2970–2980, 2010. b. DOI: 10.1016/j.rse.2010.08.003. Available at: https://linkinghub.elsevier.com/retrieve/pii/S0034425710002336.

VERBESSELT, Jan; ZEILEIS, Achim; HEROLD, Martin. Near real-time disturbance detection using satellite image time series. **Remote Sensing of Environment**, v. 123, n. Turner 2010, p. 98–108, 2012. DOI: 10.1016/j.rse.2012.02.022. Available at: https://linkinghub.elsevier.com/retrieve/pii/S0034425712001150.

VISCARRA ROSSEL, R. A. et al. A global spectral library to characterize the world's soil. **Earth-Science Reviews**, v. 155, n. February, p. 198–230, 2016. DOI: 10.1016/j.earscirev.2016.01.012. Available at: http://linkinghub.elsevier.com/retrieve/pii/S0012825216300113.

WULDER, Michael A.; MASEK, Jeffrey G.; COHEN, Warren B.; LOVELAND, Thomas R.; WOODCOCK, Curtis E. Opening the archive: How free data has enabled the science and monitoring promise of Landsat. **Remote Sensing of Environment**, v. 122, p. 2–10, 2012. DOI: 10.1016/j.rse.2012.01.010. Available at: http://dx.doi.org/10.1016/j.rse.2012.01.010.

SECOND PART

ARTICLE 1: HYDROPEDOLOGICAL CONFIGURATION OF THE TEMPORAL RESPONSE PATTERNS OF SOIL MOISTURE TO RAINFALL IN HILLSLOPE CLAY-SOILS

Article elaborated according to NBR 6022 standards (ABNT, 2003).

HYDROPEDOLOGICAL CONFIGURATION OF THE TEMPORAL RESPONSE PATTERNS OF SOIL MOISTURE TO RAINFALL IN HILLSLOPE CLAY-SOILS

ABSTRACT

Temporal variability of soil water content is an important indicator of the state of hydrologic systems, assisting in prediction and modeling of hydrological processes. Studies involving long-daily time series of moisture in the soil profile are still scarce in tropical environments. Temporal pattern of soil moisture response to rainfall of clay-soils and its relationship with its hydropedological setting was investigated. Six profile-probe capacitive sensors were set up at different landscape positions and soil depths in Typic Rhododult and Typic Hapludult soils under pasture and reforestation covers. Rainfall and soil moisture time series were constructed with daily data of the period from 08/2014 to 03/2018. Soil samples were collected from the soil profile at each analyzed location to provide support to the interpretation of the soil moisture time series, and, in conjunction with topographic variables, for the definition of hydropedologic units (HPUs). Temporal cross-correlation analysis between rainfall and soil moisture time series was applied for each soil depth and HPU. Surficial soil layers showed higher soil moisture variability among the analyzed sites. Taxonomic similarity of HPUs is reflected in a global pattern of soil moisture: higher water retention and decreasing variability in depth. Despite such similarity, response patterns of soil moisture to rainfall at the daily scale were found to be variable. Cross-correlations between soil moisture and rainfall were weak but significant in the majority of HPUs and soil depths ($P < 0.05$), having its temporal signature conditioned by the hydropedologic context, i.e. the conjunction of land surface and soil hydro-physical properties related to water accumulation, lateral flux, and water retention.

Keywords: Time series analysis. Soil water content. Soil hydro-physical properties. Precipitation.

1 INTRODUCTION

Soil moisture exerts an important role in many hydrological and ecological processes, as water infiltration, percolation, and runoff (CORRADINI, 2014), plant growth, and ecosystems dynamics (SANDVIG; PHILLIPS, 2006), reflecting on climate and meteorological conditions (SENEVIRATNE et al., 2010). Understanding the response patterns of soil moisture is of great importance for a wide range of disciplines and practical applications (VEREECKEN et al., 2008).

Analyzing the response of moisture and its variability in the soil profile through “in situ” monitoring of the balance of water input and output assists in understanding processes connected with water balance on large scales. Such information is fundamental for hydrological modeling and prediction, restoration of vegetation, and sustainability of soil use (WANG et al., 2014; LI et al., 2015). Non-destructive methods, based on the dielectric constant of the soil, such as time-domain reflectometry (TDR) or frequency domain reflectometry (FDR), have been extensively used for continuous monitoring of “in situ” soil moisture and to measure and model its evolution in geographic and time frames (ROMANO, 2014).

Many factors control the variability of soil moisture, remarkably: soil properties, climate, vegetation cover, and topography (GEROY et al., 2011; ROSENBAUM et al., 2012; ROMANO, 2014). Recent studies have been performed on the geographic-time variability of soil moisture and the factors that affect it throughout the world, which has shown contrasting results. The soil moisture response pattern and the effects of soil properties, vegetation, and topography on water content in the soil seems to be dependent on the climate conditions and the seasonality of meteorological events (JAMES et al., 2003; LAWRENCE; HORNBERGER, 2007; LI; RODELL, 2013). In arid and semi-arid regions, the geographic-time variation of soil moisture seems to be controlled mainly by soil properties and vegetation (CANTON; SOLE-BENET; DOMINGO, 2004; COSH et al., 2008; LI et al., 2015, MELO; MONTENEGRO, 2015). However, Li et al. (2017) observed that dynamic factors as rainfall exerted greater control on soil moisture variation in the time dimension in a humid climate region. Kim and Barros (2002), and Oldak, Jackson and Pachepsky (2002) reported that the spatial variability of soil moisture was predominantly controlled by rainfall patterns under moist conditions and by the soil texture and vegetation under dry conditions.

Soil moisture variability is also regulated by the mean moisture content in the soil (FAMIGLIETTI et al., 2008; ROSENBAUM et al., 2012). Many studies have shown an inverse relationship between soil moisture variability and mean soil water content (FAMIGLIETTI et

al.,1999; LAWRENCE; HORNBERGER, 2007), while there are also reports of greater variability as the mean moisture content increases (e.g. LAWRENCE; HORNBERGER, 2007; MARTÍNEZ-FERNÁNDEZ; CEBALLOS, 2003), such facts highlight the complexity of analyzing soil moisture in a temporal frame. A range of contrasting information regarding the effects of vegetation cover (WANG et al., 2014; WANG et al., 2015), climate (TEULING et al., 2007), soil properties (MARTINEZ; PACHEPSKY; VEREECKEN, 2014), and topography (HAWLEY; JACKSON; McCUEN, 1983) on the dynamics of soil moisture is available in the literature.

Given that the information on soil moisture from specific sites can be extrapolated across the landscape, observations must be linked to soil properties (PAN et al., 2012). Hydropedologic attributes, i.e., those related to water storage and redistribution processes in the soil, such as soil texture and particle size distribution (BHARALI, 2019), and those attributes related to water retention (GEROY et al., 2011), hydraulic conductivity (OJHA et al., 2017), and soil depth (MENEZES et al., 2009) have proven to be fundamental in the interpretation of the response of water content in the soil profile; as well as its application in mathematical models that attempt to describe and understand water dynamics in the soil-plant-atmosphere system (PREVEDELLO et al., 2007). Such a complex interaction among the diverse factors in the geographic-time frame of soil moisture reinforces the importance of the analysis of soil moisture patterns under different hydropedological configurations.

While a considerable advance in the field of monitoring soil moisture in tropical environments, counting in studies developed on multiple geographic and time scales has been made (ÁVILA et al., 2010a, 2010b, 2011; LEITE et al., 1997; MELO; MONTENEGRO, 2015; PREVEDELLO et al., 2007; SENA et al., 2017) research involving daily time series analysis of soil moisture at different depths is still scarce (BRUNO et al., 2006; JUHÁSZ et al., 2006). Furthermore, there are no reports of studies involving daily time series of soil water content in tropical mountain clay-soil profiles in Brazil, such as those occurring in the Serra da Mantiqueira region. In this sense, this study aimed to investigate the hydropedologic configuration that influences the temporal variation of soil moisture as a response to rainfall in a tropical hillslope.

2 MATERIAL AND METHODS

2.1 Study area

The study sites are located in the Posses watershed which belongs to the Cantareira Water Supply System, located in the Extrema municipality, Minas Gerais, southern Brazil (FIGURE 1). This area is part of the Serra da Mantiqueira range, presenting steep slopes and complex topography, in which the altitude ranges from 945 to 1435 m. According to the Köppen classification system, the climate is classified as Cfb: mesothermal without a dry season, and a hot summer (ALVARES et al., 2013). The mean annual temperature is 18 °C, the hottest and coldest months presents average temperatures of 25.6 °C and 13.1 °C, respectively. The average annual rainfall is 1,447 mm. The wettest three months span from December to February, while driest months are from June to August (ALVARES et al., 2013).

Figure 1 – A) Location of the study area, B) soil moisture (SM) monitoring sites, and digital elevation model in the Posses watershed. Coordinate system UTM-23 K, Datum WGS84.

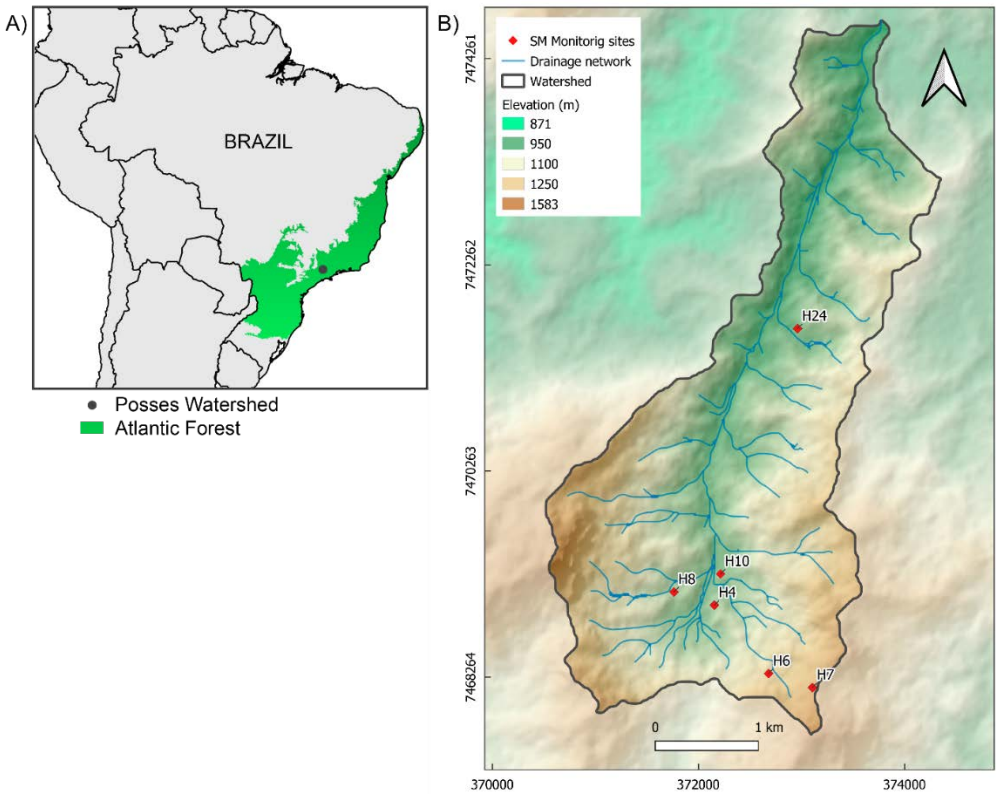

Source: From the author.

The soil parent material is granite (CPRM, 2003), with a predominance of Typic Rhododult (56 %) and Typic Hapludult (22 %) soils, which corresponds to the Red Argisol and Red-Yellow Argisol classes in the Brazilian Soil Classification System, respectively (SILVA et al., 2019). Extensive dairy farming is the predominant activity since hilly topography hinders other agricultural activities. Extensive pastures occupied around 88% of the area (LIMA et al. 2016; SAAD et al., 2018). However, since 2013, pasture has gradually been replaced by

reforestation patches of native species. This watershed is also a pilot project in the “Water Conservation” initiative that has been established in 2006 to implement the payment for ecosystem services in Brazil (PEREIRA *et al.,* 2010), aiming to ensure fresh-water resources for Cantareira Water Supply System, the main water provision basin of the metropolitan region of São Paulo. It is also a strategy for increasing the forest cover of the Rio Jaguari drainage basin (AVANZI et al., 2011).

2.2 Soil moisture and rainfall monitoring systems

Rainfall time series (R-TS) were built based on averaged daily records of seven rain gauges located across the study watershed, for the period from August - 2014 to March - 2018.

Six capacitive sensors of the PR2/6 profile-probe type (Delta T Devices, UK) associated with data loggers were installed in Typic Rhododult and Typic Hapludult soils (Figure 1B). The sensors registered soil moisture in every 5 minutes at the following soil depths: -10, -20, -30, -40, -60, and -100 cm. The sensors were previously calibrated in the laboratory for the specific conditions of the soils monitored from undisturbed samples collected in the study area; the detailed procedure and calibration equations can be found in Silva (2019). Five sensors were set up in extensive pasture areas, and one sensor was set up in a reforestation area, established in 2013 with native species. Averaged daily values of soil moisture were used for creating soil moisture time series (SM-TS).

2.3 Hydropedological characterization of the monitoring sites

Each monitoring site was interpreted as a hydropedologic unit (HPU). HPU characterization involved the collection of disturbed and undisturbed soil samples from the 0 - 20, 20 - 40, 40 - 60, and 60 - 100 cm layers, making up three subsamples per layer. Soils collected were analyzed to determine the following hydropedologic attributes: textural fractions, soil bulk density, organic matter, macro- and micro-porosity, total porosity, and soil water retention parameters.

To determine the soil moisture at field capacity (10 kPa) and permanent wilting point (1500 kPa), the undisturbed samples were initially saturated and subjected to matric potentials of 10 kPa, using the Buchner funnel suction units, and of 1500 kPa in the Richards extractor. After stabilization, the samples were weighed wet and then placed in a laboratory oven at 105 ºC for 24 hours. The moisture obtained on a gravimetric basis was converted to a volumetric basis from the soil bulk density obtained for each soil layer.

The topographic characterization of each HPU was based on a set of terrain attributes derived from an ALOS - PALSAR digital elevation model (DEM) of 12.5 m of spatial resolution. From DEM, other terrain attributes were generated: topographic wetness index, topographic position index, slope, direct isolation, and diffuse isolation; which were obtained in the SAGA-GIS software (CONRAD et al., 2015). Subsequently, a buffer of two nearest pixels around each monitored location was used, generating a total of nine pixel-values per each HPU.

2.4 Principal component analysis

Hydropedologic attributes were submitted to principal component analysis (PCA), having each soil layer as an individual, with HPU as a supplementary categorical variable. Logarithmic transformation was performed, since the variables are ratio data. Terrain attributes were also submitted to PCA, but with the nearest pixel-values as individuals in addition to its location sites, and HPU as a supplementary categorical variable. Both datasets were scaled to unit variance, and PCA was based on its correlation matrices.

2.5 Rainfall time series analysis

R-TS was submitted to a 'pre-whitening' process before cross-correlation analysis between soil moisture and rainfall. This procedure aimed to remove the trend and seasonal components from the R-TS, by assuming the model in Equation 1. Once removed, temporal cross-correlation was analyzed between SM-TS segments, and residual R-TS (e_t) at each soil depth and HPU: $ccf\,(\theta_{t+k}, R_t)_{ij}$; being that *ccf* is the cross-correlation function, θ_t and R_t are the soil moisture segments and rainfall residual time series, *k* is the time lag, and *i* and *j* are indices for soil depth and hydropedologic unit, respectively.

$$Y_t = T_t + S_t + e_t \qquad (1)$$

Where, Y_t: observed data at time t, T_t: trend component, S_t: seasonal component, and e_t: residual component.

2.5.1 Data filtering

Due to the presence of large gaps in SM-TS, a selection of the longest continuous segments was necessary for each HPU. Subsequently, overlapping segments between SM-TS and R-TS were generated and analyzed.

PCA, pre-whitening, and cross-correlation analysis were performed by R software (R-CORE-TEAM, 2019) packages '*FactoMineR*' (LÊ; JOSSE; HUSSON, 2008), '*BFAST*' (VERBESSELT et al., 2010a, 2010b), '*astsa*' (STOFFER, 2019), and '*MASS*' (VENABLES; RIPLEY, 2002) .

3 RESULTS

3.1 Soil moisture variability

Figure 2 displays the boxplot analysis of soil moisture by depth in each HPU. In general, the variability of the analyzed SM-TS segments was higher in the surface layers and decreased down the soil profile, at the same time that median soil moisture increased (Figure 2), which is frequently observed in similar studies (JIA et al., 2013; LI et al., 2017; NEVES et al., 2017; ROSENBAUM et al., 2012; TAKAGI; LIN, 2011).

In both Figures 2 and 3, it is possible to notice high SM variations at the depths of 10 and 20 cm in the majority of HPUs. The data of the H24 station shown many atypical values, notably in the -60 cm layer, which can be artifacts in the dataset.

Figure 2 – Boxplots of extracted segments of volumetric soil moisture by depth and monitoring hydropedologic unit in the Posses watershed.

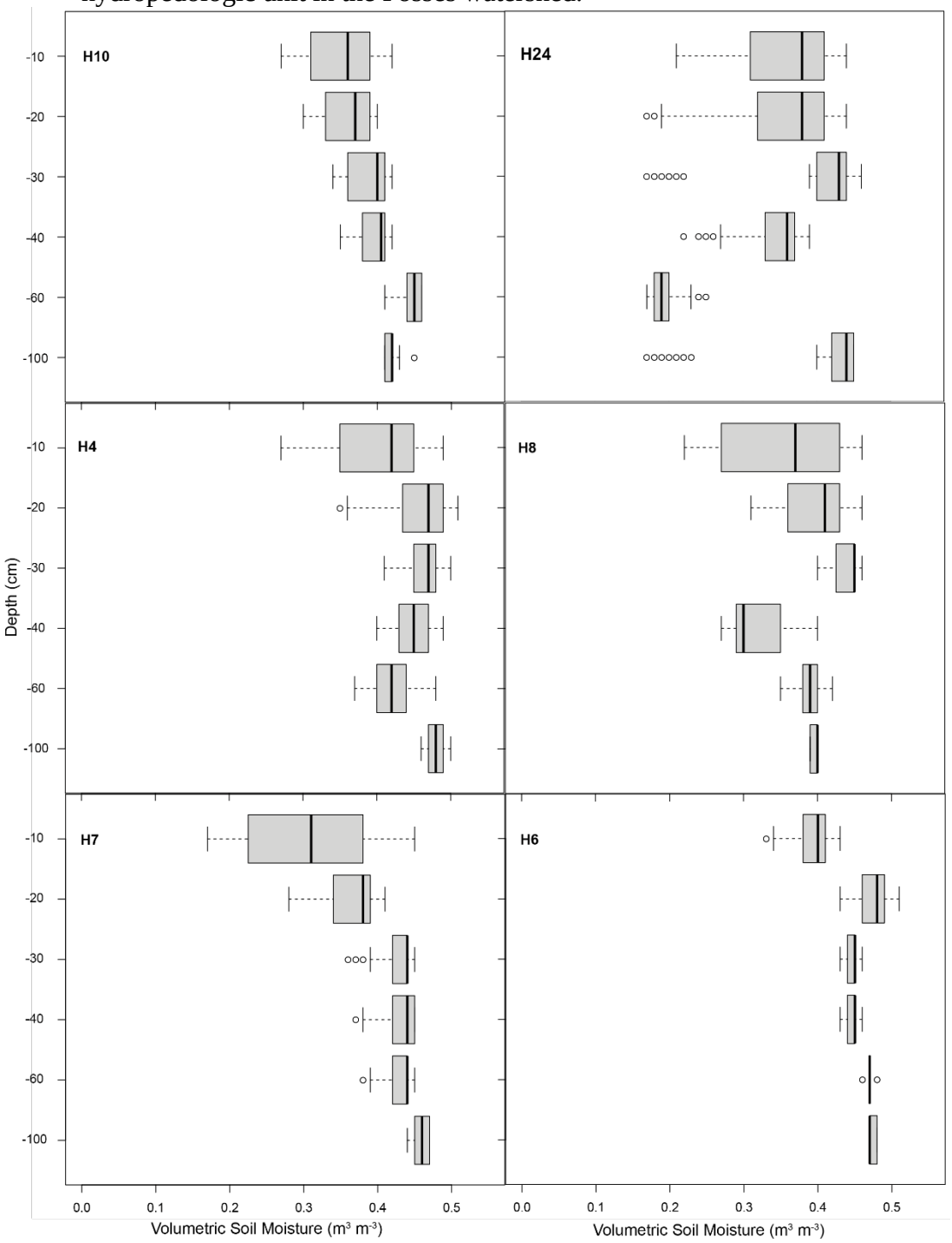

Source: From the author.

Figure 3 – Extracted segments of rainfall and soil moisture used for cross-correlation analysis at each hydropedologic unit in the Posses watershed. X-axis units are in decimal years.

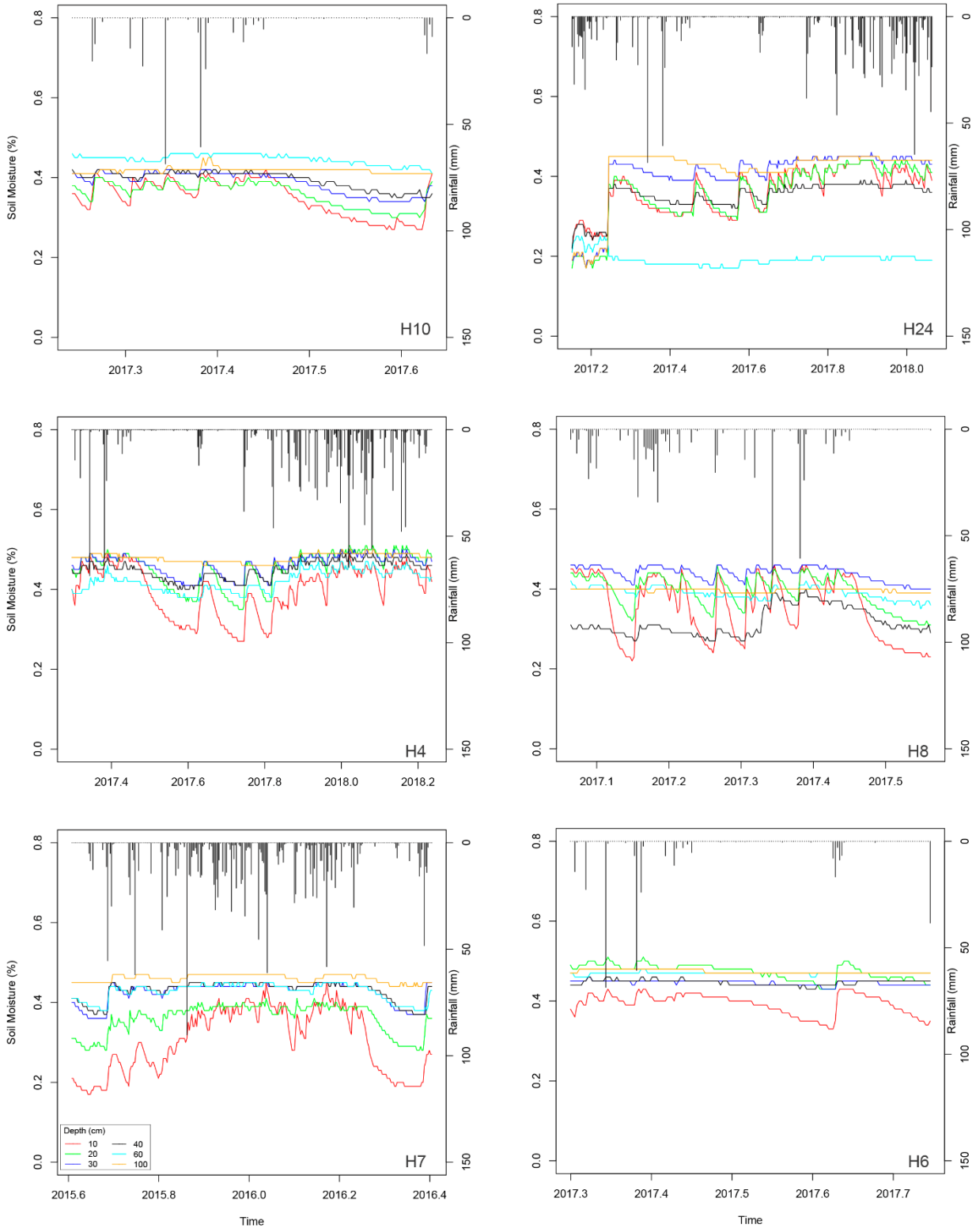

Source: From the author.

Continuous and overlapping time series segments of rainfall and soil moisture are displayed in Figure 3, from which can be verified that temporal soil moisture patterns, in all the analyzed depths and HPUs, exhibited a very similar temporal signature following a vertical variation down the analyzed profiles, where the soil moisture signals exhibit a decrease in amplitude with no observable phase delay, particularly in depths higher than 20 cm. At the depth of 100 cm, soil moisture was practically constant in all HPUs (Figure 3). At such depth, soil moisture remained high throughout the analyzed time series segments and remained near or above the water contents at field capacity (FC), which has an average soil moisture value of 35 % (Table 1).

3.2 Hydropedologic configuration

Hydropedologic configuration was defined and interpreted based on two contexts: soil and landscape. The soil context accounted for physical and hydric attributes related to surface and subsurface water dynamics, while the landscape context consisted of terrain attributes linked to water dynamics.

According to Figure 4A, strong relationships among soil properties were found, expressing 76% of total inertia in the dataset. This could be considered a significant synthesis of data variability, accounting for 49% for the 0.95 quantile of an equivalent random dataset (HUSSON; LÊ; PAGÈS, 2017). Figure 4B shows that the first axis of PCA (Dim 1) strongly opposes H4, H10, H8, and H6 (to the right of the graph, characterized by a strongly positive coordinate) to H7 and H24 (to the left of the graph, characterized by a strongly negative coordinate). As a group characterized by a positive coordinate on the PC 1 axis, the HPUs H8 and H4 shared higher values of total porosity, clay content, and microporosity (variables are sorted from the strongest correlation), and low values of soil bulk density. H10 and H6 shared higher values for the variables permanent wilting point, field capacity, and microporosity (variables are sorted from the strongest correlation) and lower values of macroporosity. Finally, H24 and H7 presented higher values of soil bulk density, and lower values of microporosity, PWP, FC, and clay content (variables are sorted from the weakest correlation).

The second biplot axis in Figure 4B (Dim 2) opposes H8 and H4 (to the top of the graph, characterized by a strongly positive coordinate on the axis) to H10 and H6 (to the bottom of the graph, characterized by a strongly negative coordinate on the axis). The group of H8 and H4 (characterized by a positive coordinate on the axis) is sharing higher values for the variables TP, clay content, macroporosity (variables are sorted from the strongest), and low values for

the variable SBD. The group of H10 and H6 (characterized by a negative coordinate on the axis) is sharing high values for the variables PWP, FC, and microporosity (variables are sorted from the strongest), and low values for the variable macroporosity.

Table 1 – Characterization of analyzed hydropedologic units.

HPU	Soil type	Vegetation cover	Soil layer (cm)	Texture class	SBD (g cm^{-3})	SOM (dag kg^{-1})	TP (%)	FC (%)	PWP (%)
H7	Typic Rhododult	Pasture	0 - 20	Clay loam	1.23	40.2	49.0	30.7	24.6
			20 - 40	Clay loam	1.39	16.7	49.6	31.7	25.2
			40 - 60	Clay loam	1.31	8.9	50.3	32.6	25.8
			60 - 100	Clay	1.22	7.4	50.3	32.6	25.8
H6	Typic Rhododult	Pasture	0 - 20	Clay	1.22	27.7	52.3	36.6	29.7
			20 - 40	Clay	1.20	14.4	53.8	35.7	29.2
			40 - 60	Clay	1.32	9.8	55.2	34.8	28.6
			60 - 100	Clay	1.38	5.7	55.2	34.8	28.6
H4	Typic Hapludult	Reforestation	0 - 20	Clay	1.07	98.7	67.1	40.8	31.8
			20 - 40	Clay	1.14	7.9	62.0	39.2	32.2
			40 - 60	Clay	0.96	5.4	56.9	37.5	32.5
			60 - 100	Clay	0.99	2.6	56.9	37.5	32.5
H10	Typic Rhododult	Pasture	0 - 20	Clay loam	1.30	23.6	55.6	39.6	31.1
			20 - 40	Clay loam	1.24	11.5	54.2	40.2	32.5
			40 - 60	Clay	1.24	8.2	52.8	40.8	33.8
			60 - 100	Clay	1.16	6.8	52.8	40.8	33.8
H8	Typic Rhododult	Pasture	0 - 20	Clay	1.03	19.8	55.2	-	-
			20 - 40	Clay	1.00	12.3	60.1	-	-
			40 - 60	Clay	0.96	10.5	65.1	-	-
			60 - 100	Clay	0.95	5.7	65.1	-	-
H24	Typic Rhododult	Pasture	0 - 20	Clay loam	1.26	28.5	56.8	30.5	22.5
			20 - 40	Clay	1.28	18.2	55.3	28.6	21.6
			40 - 60	Clay	1.32	12.0	53.8	26.7	20.7
			60 - 100	Clay	1.27	9.8	53.8	26.7	20.7

HPU: hydropedologic unit, SBD: soil bulk density, SOM: soil organic matter, TP: total porosity, FC: field capacity, PWP: permanent wilting point. Source: From the author.

Figure 4 – A) Correlation between soil hydric attributes and the first two principal components after logarithmic transformation. B) Scatter of the hydric attributes of each hydropedologic unit on the biplot.

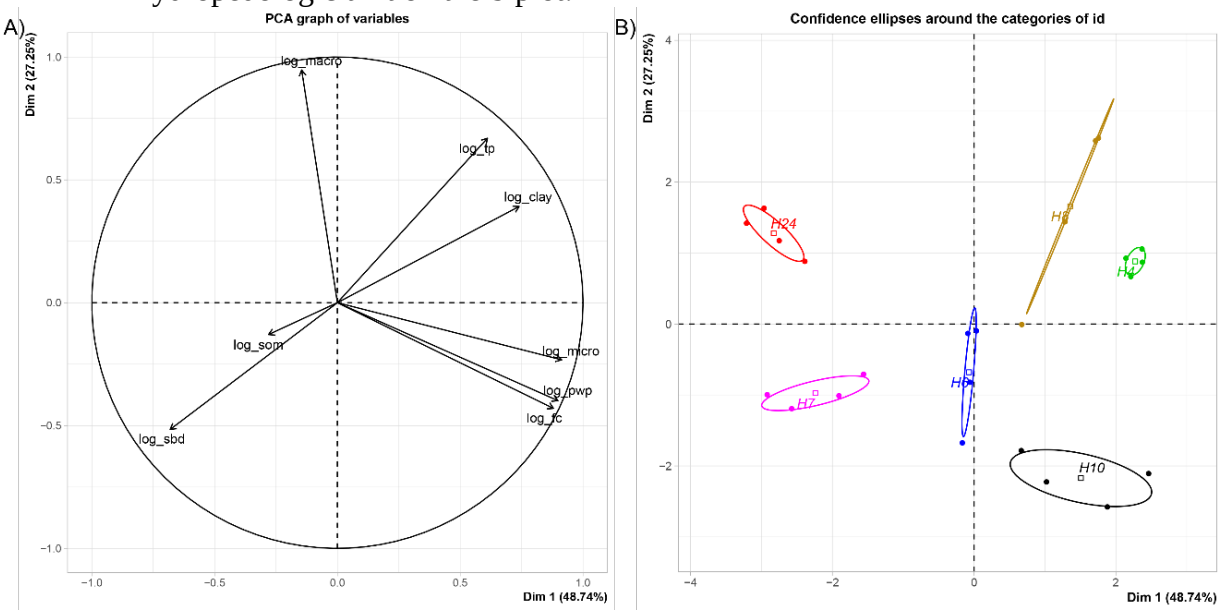

sbd: soil bulk density, som: soil organic matter, fc: soil moisture at field capacity (10 kPa), pwp: soil moisture at permanent wilting point (1500 kPa), micro: microporosity, tp: total porosity, macro: macroporosity. Each point represents a soil layer and ellipses show the 95 % confidence interval for each HPU centroid. Source: From the author.

Figure 5 - A) Correlation between terrain attributes and the first two principal components. B) Scatter of the hydric attributes of each hydrologic unic (HPU) on the.biplot.

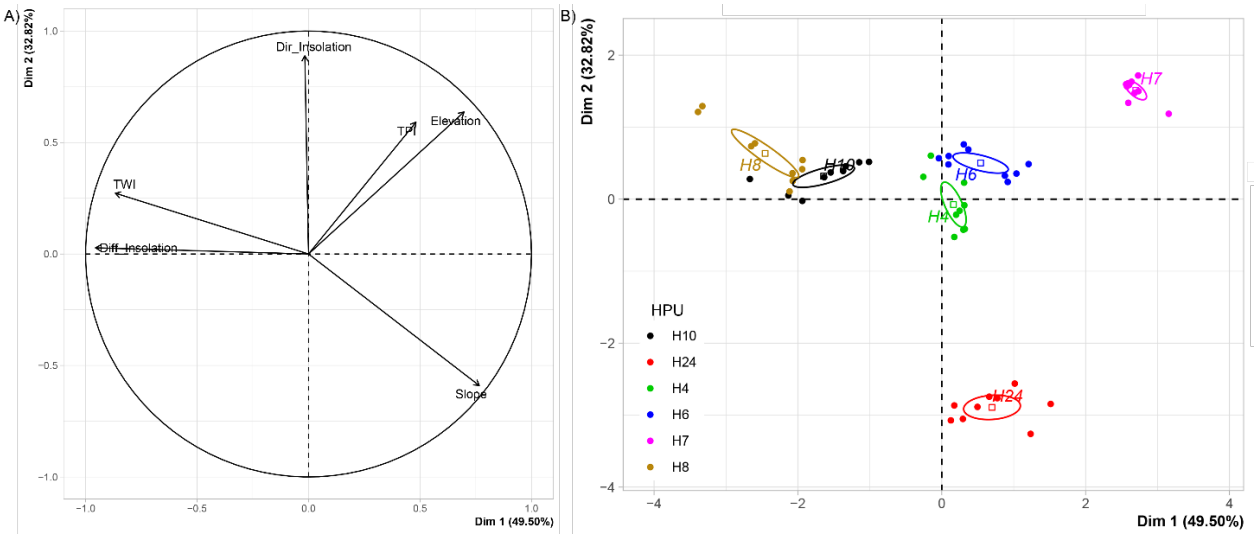

TWI: topographic wetness index, TPI: topographic position index. Ellipses show the 95 % confidence interval for each HPU centroid. Source: From the author.

Regarding topographic attributes, the first dimension inertia shows strong relationships among variables analyzed, suggesting that two dimensions should be enough in this case. The

first two dimensions express 82% of the total dataset inertia (82 % of the total variability is explained by the plane) (Figure 5). This percentage is high and thus the first plane represents an important part of the data variability. Furthermore, this value is greater than the reference value of 49%, thus, the variability explained is considered highly significant (the reference value is the 0.95-quantile of the inertia percentages distribution obtained by simulating 2248 data tables of equivalent size, based on a normal distribution).

An estimation of the right number of the axis to interpret suggests restricting the analysis to the description of the first two axes. These axes present an amount of inertia greater than those obtained by the 0.95-quantile of random distributions (82% against 49%). This observation suggests that only these axes are carrying significant information. Consequently, only these axes were described.

The first principal component (Dim 1) opposes H7 (to the right of the graph, characterized by a strongly positive coordinate on the axis) to H8 (to the left of the graph, characterized by a strongly negative coordinate on the axis). The H7 group, characterized by a positive coordinate on the axis, is sharing: higher values for the variables elevation, topographic position index, and direct insolation (variables are sorted from the strongest), and low values for the variables diffuse insolation (Diff-I and topographic wetness index (TWI; variables are sorted from the weakest). The group of H8, characterized by a negative coordinate on the axis, is sharing: higher values for the variables Diff-I, TWI, and Dir-I (variables are sorted from the strongest), and low values for the slope and elevation variables (sorted from the weakest). It is worth to note that the variable Diff-I is highly correlated with this dimension (correlation of 0.91). This variable could, therefore, summarize itself in dimension 1 (Figure 5B).

The second principal component (Dim 2) opposes H7 and H8 (to the top of the graph, characterized by a strongly positive coordinate on the axis) to H24 (to the bottom of the graph, characterized by a strongly negative coordinate on the axis). The H8 group, characterized by a positive coordinate on the axis, is sharing: higher values for the variables Diff-I, TWI, and Dir-I (variables are sorted from the strongest), and lower values for the slope and elevation variables (sorted from the weakest).

The group H7, characterized by a positive coordinate on the axis, is sharing: higher values for the variables elevation, TPI, and Dir-I (variables are sorted from the strongest); lower values of Diff-I and TWI (variables are sorted from the weakest). The group in which H24 stand, characterized by a negative coordinate on the axis, is sharing: higher values of slope, and lower values of Dir-I, TPI, TWI, and elevation (variables are sorted from the weakest). Note

that H24 is highly correlated with this dimension (correlation of 0.05). This variable could summarize itself in dimension 2 (Figure 5B).

3.3 Soil moisture response to rainfall

It was observed for the majority of soil depths a direct and statistically significance ($P < 0.05$), but with week response to rainfall (Figure 6). H24 showed no significant correlation at any evaluated level (Figure 6), preventing to draw any conclusive interaction. HPUs that registered significant and positive correlations showed different response delay of soil moisture to rainfall, conditioned by soil depth mainly. H4 and H8 presented the most similar response pattern (Figure 6).

From Figure 6 it is possible to observe a weak similarity response among H7, H10, and H6, where the soil moisture tends to correlate with rainfall in depth. Notably, in H10 (-100 cm) and H6 (-60 cm) that presented significant correlations until the fourth lag, and after a large gap, significant correlations were recorded between the 15 to 18 lags after a rainfall input. H7 (-100 cm) also shown significant correlations in the lowest analyzed soil layer, having a continuous response from 5 to 13 days after rainfall inputs.

Figure 6 – Temporal cross-correlation between deseasonalized rainfall and soil moisture at each depth and hydropedologic unit (HPU).

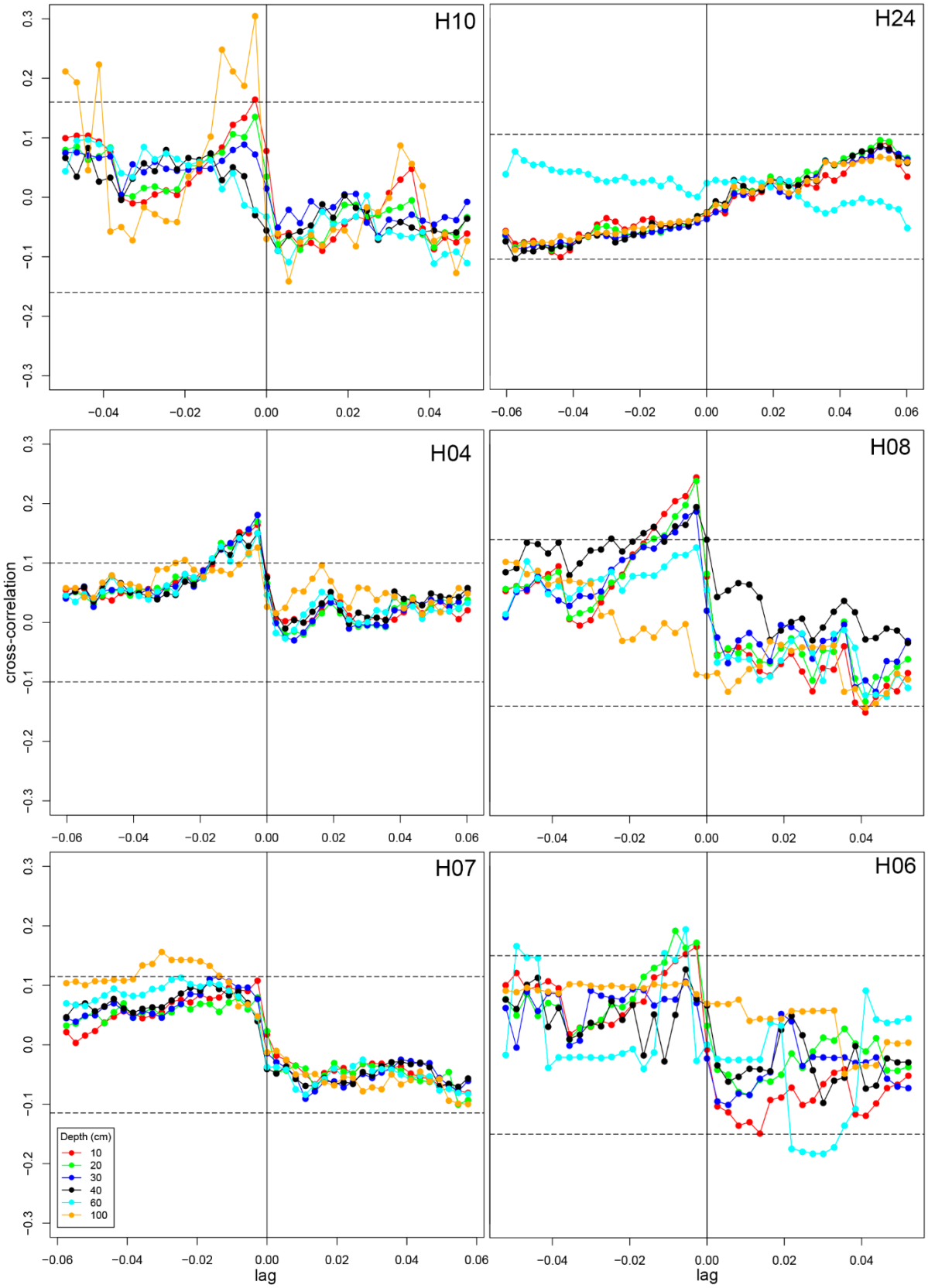

Segmented horizontal lines show 95 % confidence intervals for correlation. Source: From the author.

4 DISCUSSION

4.1 Soil moisture variability and the hydropedologic setting

The monitoring system was able to register a characteristic pattern in temporal studies of soil moisture, as a rapid increase of soil moisture due to a high matric potential in soils with low water content. It could be observed in surficial layers, due to greater exposure to atmospheric and topographic processes, controlling soil water dynamics, such as higher exposure to evapotranspiration and the direct effect of rainfall (MELO; MONTENEGRO, 2015).

Although the patterns of temporal variation among layers presented some similarity, quicker response to rainfall events and the soil drying rate collaborate to accentuated temporal variation in the soil surface layers (MELO; MONTENEGRO, 2015; ROSENBAUM et al., 2012). At the depth of 100 cm, the soil moisture time series are practically stable and similar among the six monitored locations, due to lower dependence on climatic, biological, and hydrological factors that determine soil moisture dynamics.

The signal similarity of soil moisture reflects in strong dependence on precedent soil moisture among the soil depths in the majority of monitored locations (Supplementary Figure 2), despite the differences that exist among the hydro-physical attributes of the profiles (FIGURE 4). Soils with fine texture are less prone to undergo what is called “physical decoupling of the adjacent soil layers” (CAPEHART; CARLSON, 1997). It occurs when the drying rates of the surface and under the surface diverge, controlled by the soil hydraulic properties because the changes in the moisture contents are milder in the dry seasons (VEREECKEN et al., 2008). Additionally, under conditions of higher soil moisture contents, water distribution through soil profile acts in a more homogenous way (JOST et al., 2004).

Soil moisture is higher at the surficial layers of HPU under reforestation (H4) when compared to pasture areas. Higher clay and soil organic matter contents at 0 – 20 cm depth are attributes that might strongly contribute to soil water retention (COSTA et al., 2013). Such higher organic matter content is the result of plant litter accumulation of topsoil, improving its physical conditions and soil structure (BISWAS; SI, 2011) and, consequently, promotes high soil water retention (Supplementary Figure 1).

The higher soil moisture content in the reforested area, when compared to pasture, is more evident at lower rainfall periods, where a lower decrease in moisture is observed (Supplementary Figure 2). From July to October, all the monitored sites reached lower moisture values, attaining values below its wilting point, especially in pasture areas. James et al. (2003)

also observed lower moisture values in soils under pasture when compared to those under forest and shrub vegetation in dry conditions. Similar studies also suggested that the faster drying rate of moisture in pasture areas may be related to greater demand of this vegetation for soil moisture in the surface layers (KÖCHY; WILSON 2000; MELO; MONTENEGRO, 2015; WANG et al., 2014). However, in the wettest periods, when the soil water content is higher, soil moisture tends to be less affected by vegetation, and moisture does not act as a limiting factor on evapotranspiration (ÁVILA et al., 2011; JAMES et al., 2003; MELO; MONTENEGRO, 2015; ROSENBAUN et al., 2012).

The higher water retention capacity of the Typic Rhododult and Typic Hapludult, and the high and well-distributed rainfall throughout the year, resulting in high soil moisture contents, especially at depths below 30 cm (FIGURES 2 and 3, and Supplementary Figure 2). Notwithstanding, although soil moisture contents are higher over the time series, it was not found any soil redoximorphic features that denote saturated conditions. The H7 was the only one to draw near such condition in the 100 cm layer, as a result of lower clay contents and lower total porosity (Supplementary Figure 1), which are reflected in a lower amount of water stored under saturation conditions.

Analyses in a geographic-time frame of soil moisture in arid and semi-arid regions suggest that static factors, such as texture, density, and topography, exercise greater control on soil moisture variability (COSH et al., 2008; LI et al., 2015; MELO; MONTENEGRO, 2015). However, Li et al. (2017) analyzed moisture time series in a wet climate region and observed that dynamic factors, such as rainfall, exert greater control on moisture variation in the temporal dimension. Kim and Barros (2002) and Oldak, Jackson and Pachepsky (2002) also reported that spatial variability in soil moisture was predominantly controlled by rainfall patterns under wet conditions, and by soil texture and the moisture content of vegetation under dry conditions.

Based on PCA results of land surface and soil hydro-physical attributes in first dimensions, (Figures 4 and 5), H8 and H10 showed the highest similarity, having a hydropedologic context that promotes more water retention and topographic accumulation (ZHAO et al., 2012). H7 and H24, which have higher similarity as well, their hydropedologic condition might cause less water accumulation. Finally, despite sharing a comparable topographic condition, H4, H6, and H24 are sort in the dimension of soil hydro-physical attributes, with H4 exhibiting the highest water retention capacity, H6 with a global average, and H24 with the lowest.

For most of the year, soil moisture remained near or above field capacity in the layers below 30 cm in the six monitored HPUs (Supplementary Figure 2). It is important to emphasize

that, despite the hydro-physical differences suggested by the PCA, all HPUs are expected to have high water retention capacity, which can be confirmed by the higher moisture contents at 1500 kPa tension (PWP, TABLE 1). The soil texture and specific surface of the soils exerts primary control on soil water retention capacity (HILLEL, 2003). Since the soil texture ranged from clay loam to clay and, the greater the clay content, the greater the water retention capacity (LUZ; LIMA, 2008).

Regarding the temporal interaction between soil moisture and rainfall, the expected pattern was strong and short-lag responses of soil moisture to rainfall in the topmost soil layer, reflecting in cross-correlation peaks after rainfall events, which should transfer successively down the profile as the response lag increases (MAHMOOD et al., 2011). Additionally, temporal correlation scales of soil moisture can be divided into two components: a short (event-related), which prevails in upper soil layers (-10 cm); and a long (monthly scale), prevailing in the deep layers (-100 cm) where higher scales processes (ENTIN et al., 2000). That pattern can be verified only in the H4 and H8, and partially in H6 (Figure 6). The soil surface moisture-rainfall association corroborates the coupling of near-surface atmospheric processes (MAHMOOD et al., 2011).

Soils that presented greater water retention capacity (H4, H10, and H8) should report higher cross-correlations with rainfall, as they do in coarser temporal scales (NASH et al., 1991). However, on a daily scale, the expected patterns are heavily hindered by the effects of antecedent soil moisture. Remarkably, when antecedent soil moisture has its values near to the field capacity (Table 1 and Supplementary Figure 2), the observation of a clear and direct relationship with rainfall was not possible (MONTENEGRO et al., 2018).

Additionally, Western et al., (2002) exposes that seasonal variation in soil moisture is caused by changes in the balance between potential evapotranspiration (PET) and rainfall, i.e. dry and wet seasons changes, which are part of a larger-scale process, which is followed by the changes related to the duration and intensity of discrete rainfall events. This seasonal shift between wet and dry conditions makes soil moisture consistently high or low. The balance between PET and rainfall dictates the dominant process of soil moisture dynamics in the landscape: in a less water state, local vertical fluxes predominate, which is observed in H6 and H10, with analyzed rainfall segments registered in predominantly dry conditions (Figure 3), explaining its similar response to rainfall, and lateral fluxes on the opposite state (wet), as is the case of H7, which in addition to a condition that that does not retain water, was analyzed in a wet dominating state.

Early studies carried out by Yu and Cruise (1982), and Nash et al. (1991), regarding the relationship between rainfall and soil moisture in a temporal frame, report that despite a mechanistic process of water input in the soil from rainfall exists, its evaluation by cross-correlation produces nonhomogeneous results, which is mostly caused by a significant difference in their autocorrelation structure, being higher for soil moisture than for rainfall, at a daily scale. Higher soil water retention tends to produce higher soil moisture temporal-autocorrelation, explaining a major part of the temporal variability of soil moisture, which is reflected in low values of cross-correlation with rainfall (ZHU et al., 2014).

The temporal signatures of soil moisture certainly do not reflect isolated effects of rainfall, but also other processes such as the input of exogenic soil water sourced as lateral flow and runoff from upslope areas, which in addition to the effects of antecedent soil moisture, led to the record of low to null cross-correlations. However, when registered, such signatures exhibited a clear pattern that was conditioned, at different degrees, with the hydropedologic conditions.

5 CONCLUSIONS

This study investigated the response of moisture time series to rainfall in the profile of Typic Rhododult and Typic Hapludult soils in pasture and reforested areas. Soil moisture was superior in the 10 and 20 cm soil layers in the reforested area, reflecting the better physical structure of its surficial layer, given the greater clay and organic matter contents. The variability of soil moisture was higher in the periods of lower occurrence of rains when the pasture areas reached the wilting point more frequently than the reforested area. In the layers below 30 cm, moisture remained high throughout all the time series, reflecting the high capacity of water retention and microporosity of the Typic Rhododult and Typic Hapludult soils, as well as a well-distributed rainfall. It can also be inferred a high predictability of depth soil moisture from the surface layer (-10 cm), whose pattern preserved the signal of the top-most layer with a decrease in amplitude and variability as a function of soil depth, regardless of the vegetation cover. In general, signal detection of rainfall-soil moisture relationship was hindered by its natural complexity, however despite complex interactions, a clear signal in which rainfall has a direct relationship with soil moisture was retrieved, in which the response pattern of soil moisture of the Typic Rhododult and Typic Hapludult soils is modulated by the hydropedologic setting with a variable degree, being conditioned mainly by topographic and hydro-physical variables related to water accumulation, lateral flux, and water retention.

ACKNOWLEDGMENTS

Authors recognize their gratitude to Department of Soil Science of the Federal University of Lavras (UFLA) for its support, Coordenação de Aperfeiçoamento de Pessoal de Nível Superior (Capes) - Finance code 001, for the scholarships, Programa de Excelência Acadêmica - Proex (AUXPE 593/201), Conselho Nacional de Desenvolvimento Científico e Tecnológico - CNPq (Processos 306511-2017-7 and 202938/2018-2), Fundação de Amparo a Pesquisa do Estado de Minas Gerais - FAPEMIG (Processos APQ-00802-18 and CAG-APQ 01053-15), and Fundação de Amparo à Pesquisa do Estado de São Paulo – FAPESP (ClimateWise 2015/50682-6), CAPES/ANA/ "Estimativa de evapotranspiração por sensoriamento remoto para gestão de recursos hídricos no Brasil" 88887.144979/2017-00, and CNPq/ANA 446278/2015-7 "O regime hidrológico das bacias dos Rios Piracicaba e Paraíba do Sul no clima futuro: avaliação de alta resolução dos padrões, incertezas e impactos do uso da terra" for the support and funding of this research.

REFERENCES

ALVARES, C. A. et al. Köppen's climate classification map for Brazil. **Meteorologische Zeitschrift**, Stuttgart, v. 22, n. 6, p. 711–728, 2013. doi:10.1127/0941-2948/2013/0507

AVANZI, J. C. et al. Pilot plan on groundwater recharge. Sustainable water management in the tropics and subtropics - and case studies in Brazil - Vol.1. 2011

ÁVILA, L. F.; DE MELLO, C. R.; DA SILVA, A. M. Continuidade e distribuição espacial da umidade do solo em bacia hidrográfica da Serra da Mantiqueira. **Revista Brasileira de Engenharia Agricola e Ambiental-Agriambi**, Campina Grande, v. 14, n. 12, p. 1257-1266, 2010.

ÁVILA, L. F.; MELLO, C. R.; SILVA, A. M. Estabilidade Temporal do Conteúdo de Água em três condições de uso do solo, em uma bacia hidrográfica da região da Serra da Mantiqueira, MG. **Revista Brasileira de Ciência do Solo**, Viçosa, v. 34, n. 6, p. 2001-2009, 2010.

ÁVILA, L. F. et al. Padrão Espaço-Temporal da Umidade Volumétrica do Solo em uma Bacia Hidrográfica com Predominância de Latossolos. **Revista Brasileira de Ciência do Solo**, Viçosa, v. 35, n. 5, p. 1801-1810, 2011.

BHARALI , B. Rate of infiltration for different soil textures using rainfall simulator and Green–Ampt model. **ISH Journal of Hydraulic Engineering**, London, p. 1-7, 2019.

BISWAS, A.; SI, B. C. Identifying scale specific controls of soil water storage in a hummocky landscape using wavelet coherency. **Geoderma**, Amsterdam, v. 165, p. 50-59, 2011.

BRUNO, R. D.; ROCHA, H. R.; FREITAS, H. C.; GOULDEN, M. L.; MILLER, S. D. Soil moisture dynamics in an eastern Amazonian tropical forest. Hydrological Processes, Chichester, v. 20, p. 2477-2489, 2006.

CANTON, Y.; SOLE-BENET, A.; DOMINGO, F. Temporal and spatial patterns of soil moisture in semiarid badlands of SE Spain. **Journal of Hydrology**, Amsterdam, v. 285, p. 199–214, 2004.

CAPEHART, W. J.; CARLSON, T. N. Decoupling of surface and near-surface soil water content: a remote sensing perspective. Water Resources Research, Washington, v. 33, n. 6, p. 1383–1395, 1997.

CONRAD, O. et al. System for Automated Geoscientific Analyses (SAGA) v. 2.1.4. **Geoscientific Model Develoment**, n. 8, p. 1991–2007, 2015.

CORRADINI, C. Soil moisture in the development of hydrological processes and its determination at different spatial scales. **Journal of Hydrology**, Amsterdam, v. 516, p. 1–5, 2014.

COSH, M. H.; JACKSON, T.J.; MORAN, S.; BINDLISH, R. Temporal persistence and stability of surface soil moisture in a semi-arid watershed. **Remote Sensing of Environment**, New York, v. 112, n. 2, p. 304-313, 2008.

COSTA, A. da. et al. Water retention and availability in soils of the State of Santa Catarina-Brazil: effect of textural classes, soil classes and lithology. **Revista Brasileira de Ciência do Solo**, Viçosa, v. 37, n. 6, 2013.

CPRM - SERVIÇO GEOLÓGICO DO BRASIL (2003). Mapa geológico do estado de Minas Gerais. Belo Horizonte: CPRM, 2003.

FAMIGLIETTI, J. S. et al. Ground-based investigation of soil moisture variability within remote sensing footprints during the Southern Great Plains 1997 (SGP97) Hydrology Experiment. **Water Resources Research**, Washington, v. 35, p. 1839 – 1851, 1999. doi:10.1029/1999WR900047.

FAMIGLIETTI, J. S. et al. Field observations of soil moisture variability across scales, **Water Resources Research**, Washington, v. 44, p. 1-16, 2008. doi:10.1029/2006WR00580

GAO, L.; SHAO, M. Temporal stability of shallow soil water content for three adjacent transects on a hillslope. **Agricultural Water Management**, Amsterdam, v. 110, p. 41–54, 2012. doi:10.1016/j.agwat.2012.03.012

GEROY, I. J. et al. Aspect influences on soil water retention and storage. **Hydrological Processes**, Chichester, v. 25, p. 3836–3842, 2011.

HAWLEY, M. E.; JACKSON, T. J.; MCCUEN, R. H. Surface soil moisture variation on small agricultural watersheds. **Journal of Hydrology**, Amsterdam, v. 62, p. 179–200, 1983.

HILLEL, D. **Introduction to environmental soil physics**. Cambridge: Ed. Academic press, 2003.

HUSSON, F.; LÊ, S.; PAGÈS, J. **Exploratory multivariate analysis by example using R**. 2. ed. [s.l.] Chapman & Hall/CRC, 2017.

JAMES, S. E. et al. Temporal heterogeneity of soil in grassland and forest. **Journal of Ecology**, London, v. 91, n. 2, p. 234-239, 2003.

JIA, X. X. et al. Hillslope scale temporal stability of soil water storage in diverse soil layers. **Journal of Hydrology**, Amsterdam, v. 498, n. 18, p. 254-264, 2013.

JOST, G.; SCHUME, H.; HAGER, H. Factors controlling soil water- recharge in a mixed European beech (Fagus sylvatica L.)-Norway spruce [Picea abies (L.) Karst.] stand. **European Journal of Forest Research**, v. 123, p. 93–104, 2004.

JUHÁSZ, C. E. P. et al. Dinâmica físico-hídrica de uma toposseqüência de solos sob Savana Florestada (Cerradão) em Assis, SP. **Revista Brasileira de Ciência do Solo**, Viçosa, v. 30, p. 401-402, 2006.

KIM, G.; BARROS, A. P. Space-time characterization of soil moisture from passive microwave remotely sensed imagery and ancillary data. **Remote Sensing of Environment**, New York, n. 81, p. 393–403, 2002.

KÖCHY, M.; WILSON, S. D. Competitive effects of shrubs and grasses in prairie. **Oikos**, Copenhagen, v. 91, p. 385–395, 2000.

LAWRENCE, J. E.; HORNBERGER, G. M. Soil moisture variability across climate zones. **Geophysical Research Letters**, Washington, v. 34, n. 20, p. 1-5, 2007.

LÊ, S.; JOSSE, J.; HUSSON, F. FactoMineR : An R Package for Multivariate Analysis. **Journal of Statistical Software**, v. 25, n. 1, p. 253–258, fev. 2008.

LEITE, F. P. et al. Regime hídrico do solo sob povoamento de eucalipto, floresta nativa e pastagem, na região de Guanhães-MG. **Revista Árvore**, Viçosa, v. 21, n. 4, p. 455-462, 1997.

LI, B; RODELL, M. Spatial variability and its scale dependency of observed and modeled soil moisture over different climate regions. **Hydrology and Earth System Sciences**, v. 17, p. 1177–1188, 2013.

LI, X. Z. et al. Landscape-scale temporal stability of soil water storage within profiles on the semiarid loess plateau of China. **Journal of Soils and Sediments**, Berlin, v. 15, n. 4, p. 949-961, 2015.

LI, X. Z. et al. Similarity of the temporal pattern of soil moisture across soil profile in karst catchments of southwestern China. **Journal of Hydrology**, Amsterdam, v. 555, p. 659–669, 2017.

LIMA, G. C. et al. Spatialization of soil quality index in the Sub-Basin of Posses, Extrema, Minas Gerais. Revista Brasileira de Engenharia Agrícola e Ambiental, v.20, n.1, p.78–84, 2016.

LUZ, L. R. Q. P.; LIMA, S. L. Atributos físicos e hídricos de solos em toposseqüência de tabuleiros costeiros**. Revista de Energia na Agricultura**, Botucatu, v. 23, n. 1, p. 44-59, 2008.

MAHMOOD, R. et al. Observed data-based assessment of relationships among soil moisture at various depths, precipitation, and temperature. **Applied Geography**, v. 34, p. 255–264, 2011.

MARTINEZ-FERNANDEZ, J.; CEBALLOS, A. Temporal stability of soil moisture in a large-field experiment in Spain. **Soil Science Society of America Journal**, Madison, v. 67, p. 1647–1656, 2003.

MARTINEZ, G.; PACHEPSKY, Y. A.; VEREECKEN, H. Effect of soil hydraulic properties on the relationship between the spatial mean and variability of soil moisture. **Journal of Hydrology**, Amsterdam, v. 516, p. 154–160, 2014.

MELO, R. O.; MONTENEGRO, A. A. A. Dinâmica temporal da umidade do solo em uma bacia hidrográfica no semiárido Pernambucano. **Revista Brasileira de Recursos Hídricos**, Porto Alegre, v. 20, p. 430-441, 2015.

MENEZES, M. D., et al. Dinâmica hidrológica de duas nascentes, associada ao uso do solo, características pedológicas e atributos físico-hídricos na sub-bacia hidrográfica do Ribeirão

Lavrinha-Serra da Mantiqueira (MG). **Scientia Forestalis**, Piracicaba, v. 37, n. 82, p. 175-184, 2009.

MONTENEGRO, A. A. A.; SOUZA, T. E. M. S.; SOUZA, E. R.; MONTENEGRO, S. M. G. L. Temporal dynamics of soil moisture and rainfall erosivity in a tropical volcanic archipelago. **Journal of Hydrology**, v. 563, p. 737-74, 2018.

NASH, M. S.; WIERENGA, P. J.; GUTJAHR, A. Time series analysis of soil moisture and rainfall along a line transect in arid rangeland. **Soil Science**, v. 152, n. 3, p. 189-198, 1991.

NEVES, H. H. et al. Spatial and temporal patterns of soil water content in an agroecological production system. **Scientia Agricola**, Piracicaba, v. 74, n. 5, p. 383-392, 2017.

OJHA, R. et al. Effective Saturated Hydraulic Conductivity for Representing Field-Scale Infiltration and Surface Soil Moisture in Heterogeneous Unsaturated Soils Subjected to Rainfall Events. **Water (Switzerland)**, Basel, v. 9, n. 2, p. 1-17, 2017.

OLDAK, A.; JACKSON, T. J.; PACHEPSKY, Y. Using GIS in passive microwave soil moisture mapping and geostatistical analysis. **International Journal of Geographical Information Science**, London, v. 16, n. 7, p. 681–698, 2002.

PAN, W. et al. Characterizing Soil Physical Properties for Soil Moisture Monitoring with the North Carolina Environment and Climate Observing Network. **Journal of Atmospheric and Oceanic Technology**, Boston, v. 29, n. 7, p. 933-943, 2012.

PEREIRA, P. H. et al. **Conservador das Águas, 5 anos**. Extrema: Departamento de Meio Ambiente, 2010.

PREVEDELLO, C. L. et al. Balanço de água por aquisição automática de dados em cultura de trigo (Triticum aestivum L.). **Revista Brasileira de Ciência do Solo**, Viçosa, v. 31, n.1, p. 1-8, 2007.

R-CORE-TEAM. **R: A Language and Environment for Statistical Computing,** Vienna, 2019. Available at: <www.R-project.org>

ROMANO, N. Soil moisture at local scale: measurements and simulations**. Journal of Hydrology**, Amsterdam, v. 516, p. 6-20, 2014.

ROSENBAUM, U. et al. Seasonal and event dynamics of spatial soil moisture patterns at the small catchment scale. **Water Resources Research**, Washington, v. 48, n. 10, 2012.

SAAD, S. I. et al. Analyzing ecological restoration strategies for water and soil conservation. 2018. PLoS ONE 13(2): e0192325. https://doi.org/10.1371/journal.pone.0192325

SANDVIG, R. M.; PHILLIPS, F. M. Ecohydrological controls on soil moisture fluxes in arid to semiarid vadose zones. **Water Resources Research**, Washington, v. 42, n. 8, 2006.

SENA, A. G. et al. Multivariate analysis of soil moisture data. **Journal of Hyperspectral Remote Sensing**, Recife, v. 7, p. 432-438, 2017.

SENEVIRATNE, S. I. et al. *Investigating soil moisture–climate interactions in a changing climate: a review*. **Earth-Science Reviews**, Amsterdam, v. 99, p. 99–174, 2010.

SILVA, B. P. C. et al. Digital soil mapping including additional point sampling in Posses ecosystem services pilot watershed, southeastern Brazil. **Scientific Reports**, v. 9 , n. 13763, p. 1-12, 2019.

SILVA, B. P. C. Hydropedology as support for water resources management in an experimental watershed at Mantiqueira mountain range. 2019. 92 p. Tese (Doutorado em Ciência do Solo) – Universidade Federal de Lavras, Lavras, 2019.

STOFFER, D. **astsa: Applied Statistical Time Series Analysis**, 2019. Available at: <CRAN.R-project.org/package=astsa%0A>

TAKAGI, K.; LIN, H. S. Temporal dynamics of soil moisture spatial variability in the shale hills critical zone observatory. **Vadose Zone Journal**, Madison, v. 10, p. 832–842, 2011.

TEIXEIRA, P. C. et al. Manual de métodos de análise de solo. 3ed. rev. e ampl. Brasília, DF : Embrapa, 2017

TEULING, A. J. et al. Climate variability effects on spatial soil moisture dynamics. **Geophysical Research Letters**, Washington, v. 34, n. 6, p. 2-5, 2007.

VENABLES, W.; RIPLEY, B. **Modern Applied Statistics with S**. 4. ed. New York: Springer, 2002.

VERBESSELT, J. et al. Detecting trend and seasonal changes in satellite image time series. **Remote Sensing of Environment**, v. 114, n. 1, p. 106–115, jan. 2010a.

VERBESSELT, J. et al. Phenological change detection while accounting for abrupt and gradual trends in satellite image time series. **Remote Sensing of Environment**, v. 114, n. 12, p. 2970–2980, 15 dez. 2010b.

VEREECKEN, H. et al. On the value of soil moisture measurements in vadose zone hydrology: a review. **Water Resources Research**, Washington, v. 46, n. 4, p. 1-21, 2008.
ZHAO, Y. et al. Hydropedology in the ridge and valley: Soil moisture patterns and preferential flow dynamics in two contrasting landscapes. In: LIN, H (Ed.). **Hydropedology: Synergistic integration of soil science and hydrology**. Academic Press, Waltham, MA, 381-411, 2012.
ZHU, Q.; NIE, X.; ZHOU, X.; LIAO, K.; LI, H. Soil moisture response to rainfall at different topographic positions along a mixed land-use hillslope. Catena, n. 119, p. 61–70, 2014.

WANG, B. et al. Vertical profiles of soil water content as influenced by environmental factors in a small catchment on the hilly-gully Loess Plateau. **PLoS One**, San Francisco, v. 9, n. 10, p. 17-20, 2014.

WANG, Y. Q. et al. Vertical distribution and temporal stability of soil water in 21-m profiles under different land uses on the Loess Plateau in China. **Journal of Hydrology**, Amsterdam, v. 527, p. 543-554, 2015.

WESTERN, A. W.; GRAYSON, R. B.; BLÖSCHL, G. Scaling of soil moisture: A hydrologic perspective. **Annual Review of Earth and Planetary Sciences**, 8(30):149-80, 2002.

YU, S. L.; CRUISE, J. F. Time series analysis of soil moisture data. Developments in Water Science, v. 17, p. 600-607, 1982.

Supplementary Figure 1 – Soil profile hydro-physical attributes of the analyzed hydropedological units.

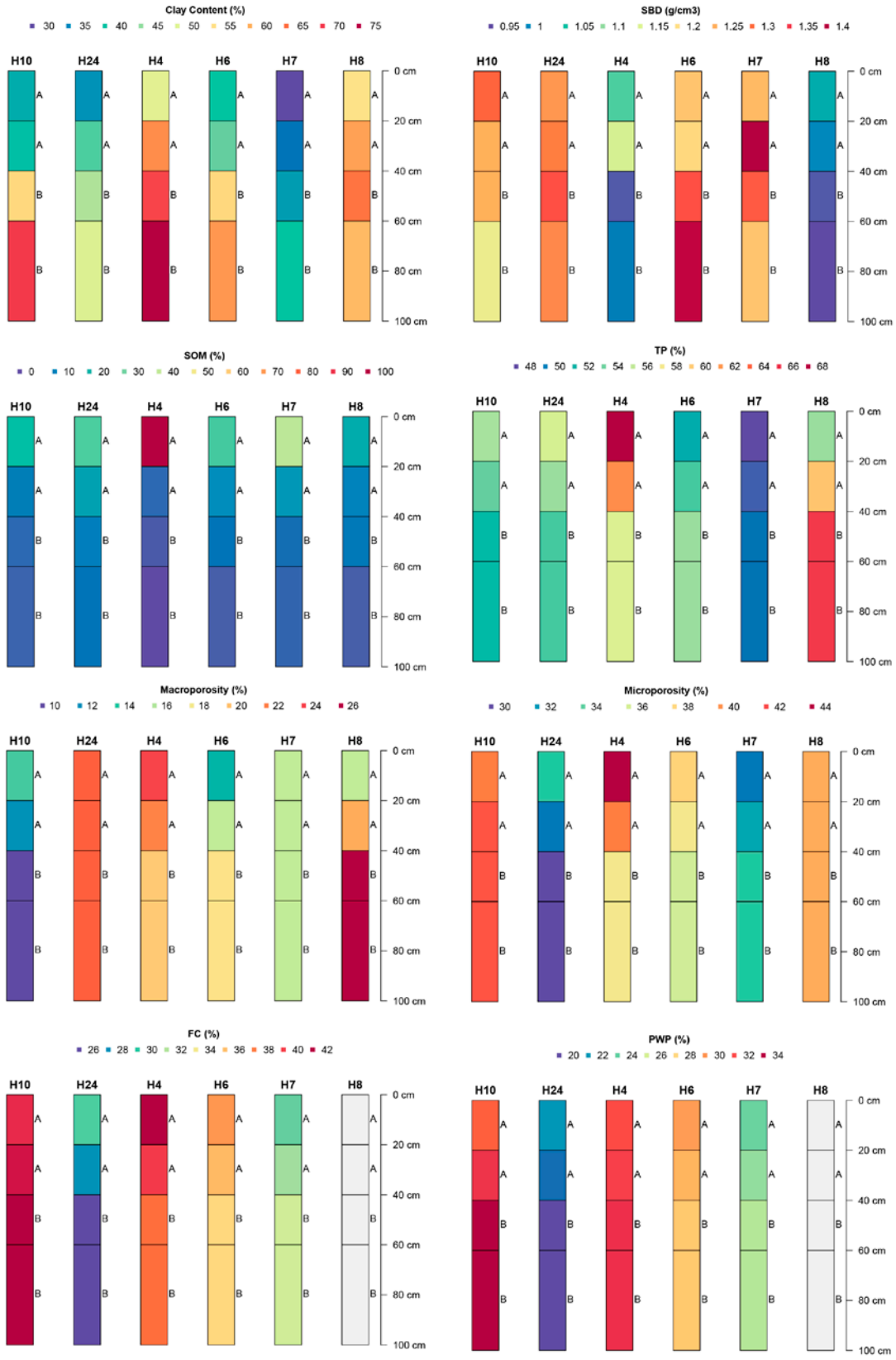

SBD: soil bulk density, SOM: soil organic matter, TP: total porosity, FC: soil moisture at field capacity (10 kPa), PWP: soil moisture at permanent wilting point (1500 kPa), FC and PWP values were not measured for H8. Source: From the author.

Supplementary Figure 2 - Complete time series of soil moisture and rainfall at each hydropedologic unit (HPU).

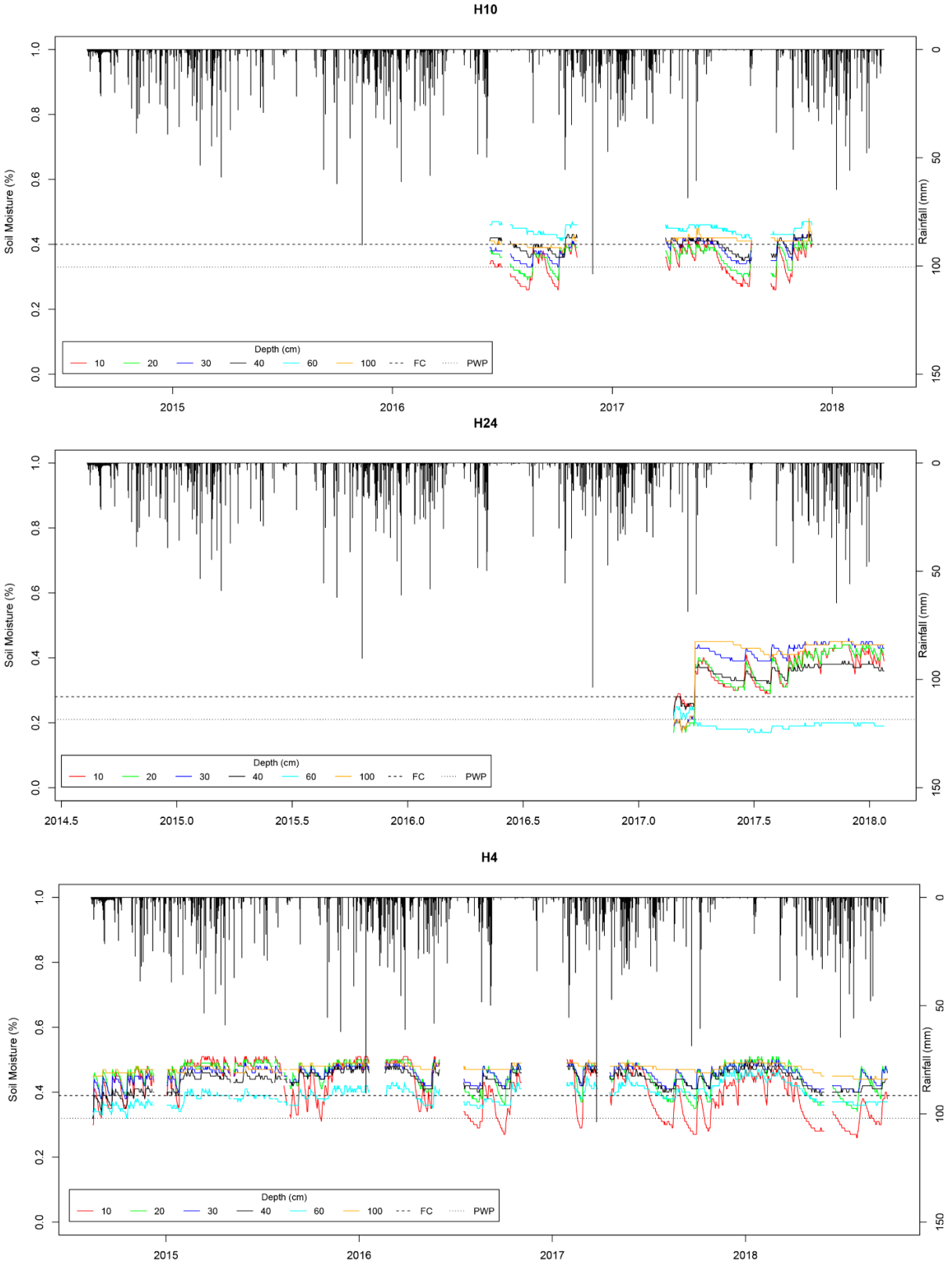

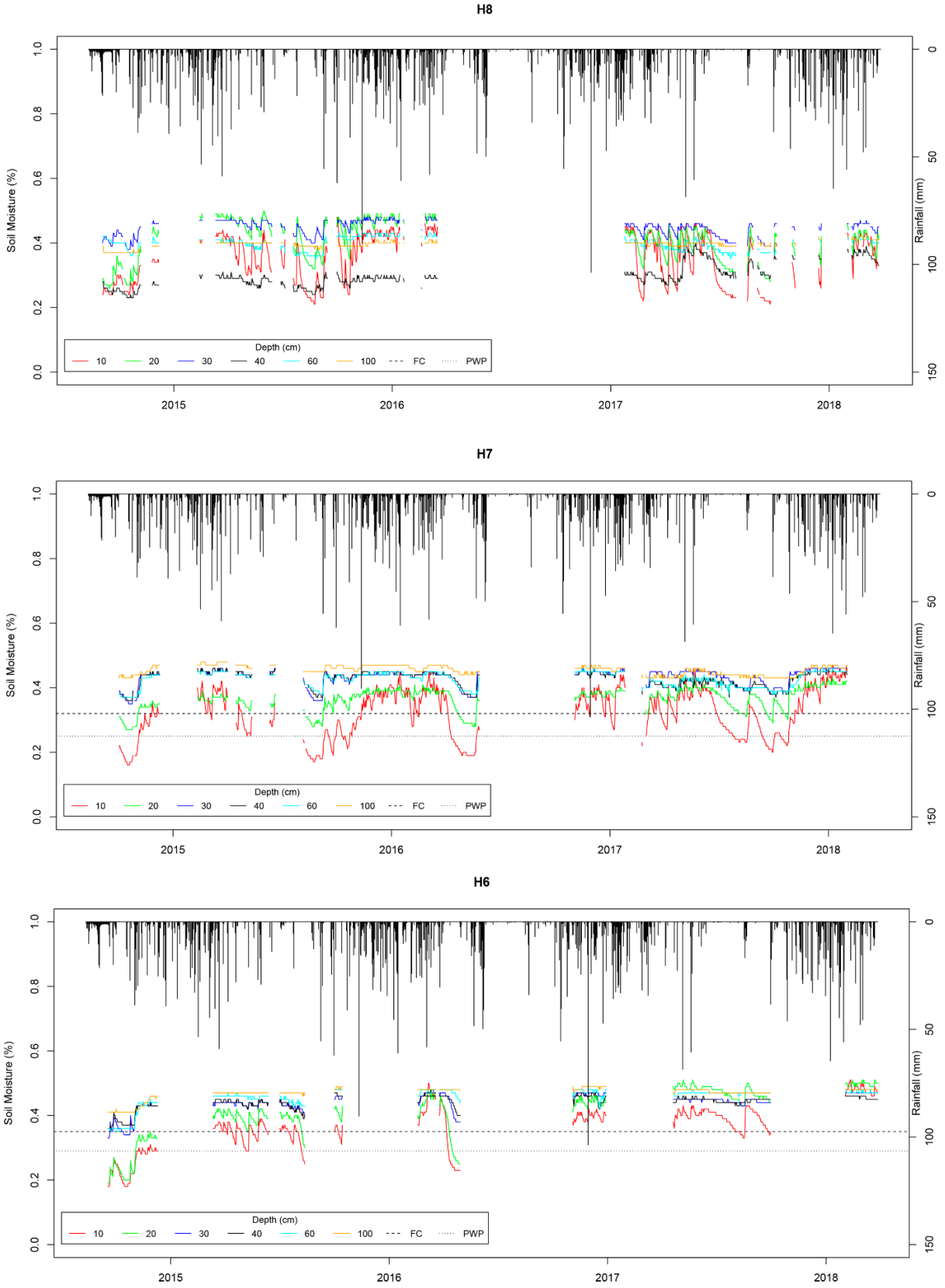

FC: average soil moisture at field capacity (10kPa), PWP: average soil moisture at permanent wilting point (1500 kPa). FC and PWP values were not measured for H8. Source: From the author.

ARTICLE 2: EVALUATION OF SYNTHETIC-TEMPORAL IMAGERY AS COVARIATES FOR DIGITAL SOIL MAPPING: A CASE STUDY IN SOILS UNDER TROPICAL PASTURE

Article elaborated according to standards of the scientific journal GIScience & Remote Sensing.

Evaluation of synthetic-temporal imagery as covariates for digital soil mapping: A case study in soils under tropical pastures

Geographic distribution of soil is related to crucial earth processes, its mapping supports modeling and planning for the conservation of ecosystems and the sustainability of agriculture. Current availability of dense time-series of surface reflectance data (SR) offers an interesting source of information for digital soil mapping (DSM), notably in regions under permanent vegetation cover. A detailed soil survey, a stack of Landsat 8 SR data, and rainfall time-series were analyzed to evaluate the influence of soil on the response of temporal patterns of vegetation greenness, assessed by the normalized difference vegetation index (NDVI). Based on such relationships, imagery depicting metrics of land surface phenology (LSP), obtained by the TIMESAT algorithm, in conjunction with other soil-forming factor proxies, were evaluated as covariates for the production of a digital soil map by applying the random forest algorithm. Four soil classes, typical of tropical regions, under pasture cover were analyzed. Covariates depicting parent material and topography recorded similar importance to LSP metrics, notably, those LSP images related to the seasonal availability of water to plants (large integrated NDVI and base NDVI value), which registered significant contributions to the random forest model (both with ~10 % of mean decrease in accuracy). Effects of rainfall seasonality on LSP were verified stronger for the Red Latosol class (Rhodic Hapludox). Results of this approach demonstrated that the addition of temporal variability of vegetation greenness can be applied to access soil subsurface processes and assists DSM.

Keywords: Vegetation greenness; NDVI; Random Forest; Land surface phenology

1. Introduction

Geographic distribution of soil is the result of a complex interaction of soil-forming factors across a continuum of spatiotemporal domains. Digital soil mapping (DSM) aims to integrate the relationships occurring over a geomorphological setting, at the landscape level, between climate and vegetation patterns into a soil map (McBratney, Mendonça Santos, and Minasny 2003; Ma et al. 2019). Vegetation, a dynamic soil-forming factor, has a strong relationship with climate and soil properties, remarkably with those that constrain plant growth and vigor, i.e. water availability and fertility (Araya et al. 2016; Fujii et al. 2018; Li et al. 2012; Berry

and Mackey 2018). As a result, spatial distribution and temporal dynamics of vegetation are indicators of the interaction between underlying soil conditions and climate regimes.

Remote sensing (RS) of vegetation greenness, a spectral feature correlated with vegetation biomass, productivity, health, and vigor, has been proved as a reliable tool for the detection and mapping of temporal and spatial dynamics of plants; being the most used technique the normalized difference vegetation index – NDVI (Helman 2018; Mulder et al. 2011; Rouse et al. 1974). As a result of the growing availability of RS data and cloud-computing, continuous collections of satellite imagery has been used to add the temporal dimension into studies using spectral vegetation indices (Padarian, Minasny, and McBratney 2015; Dwyer et al. 2018). Research on the use of temporal variability of vegetation indices (VIs) in DSM has followed different approaches, from single-season analysis, based on the comparison of wet to dry conditions (Demattê et al. 2017), to the analysis of dense time series of VIs (Maynard and Levi 2017; Li et al. 2012).

Analysis of seasonal variability of vegetation greenness retrieved by remote sensing, which is referred to as land surface phenology – LSP (Helman 2018), can also produce covariates for DSM. Using LSP metrics imagery related to vegetation growing seasons, e.g. beginning and end of seasons, integrated NDVI, and seasonal amplitudes, enable the synthesis of information depicting climate-driving cycles of vegetation greenness (Jönsson and Eklundh 2004). Nevertheless, although the feasibility of the use of LSP metrics for DSM of soil properties such as organic carbon, sand, and calcium content, was demonstrated (Yang et al. 2020; Fathololoumi et al. 2020), little attention was paid to the effects of soil taxonomic class and the interaction with rainfall seasonality, notably in tropical regions. Consequently, the objective of this study was to assess the use of LSP metrics in the production of digital soil maps. The evaluated hypothesis was that temporal variability of vegetation greenness is

conditioned by the interaction of soil taxonomic class and rainfall seasonality, which generates a ‘temporal signature’ susceptible to be retrieved by remote observation.

2. Material and methods

2.1. Study area and soil survey

A detailed soil survey was carried out based on a regularly spaced grid (~130 m of nearest neighbor distance) over an area of ~314 ha located on the Campus of Federal University of Lavras, Southern Minas Gerais state, Brazil (Figure 1), from which, soil samples from A and B horizons were collected and analyzed to determine their soil taxonomic class in agreement with the Brazilian soil classification system (Santos et al. 2018). According to Köppen's classification criteria, the climate of the region is Cwb, i.e. humid tropical with dry winter and temperate summer (Alvares et al. 2013). Based on data from the MapBiomas project, it was verified that vegetation cover is a mosaic of pasture, forest formation, forest plantation, and agriculture and it has no suffer significant land cover change between the period of 2012 - 2019 (Souza et al. 2020).

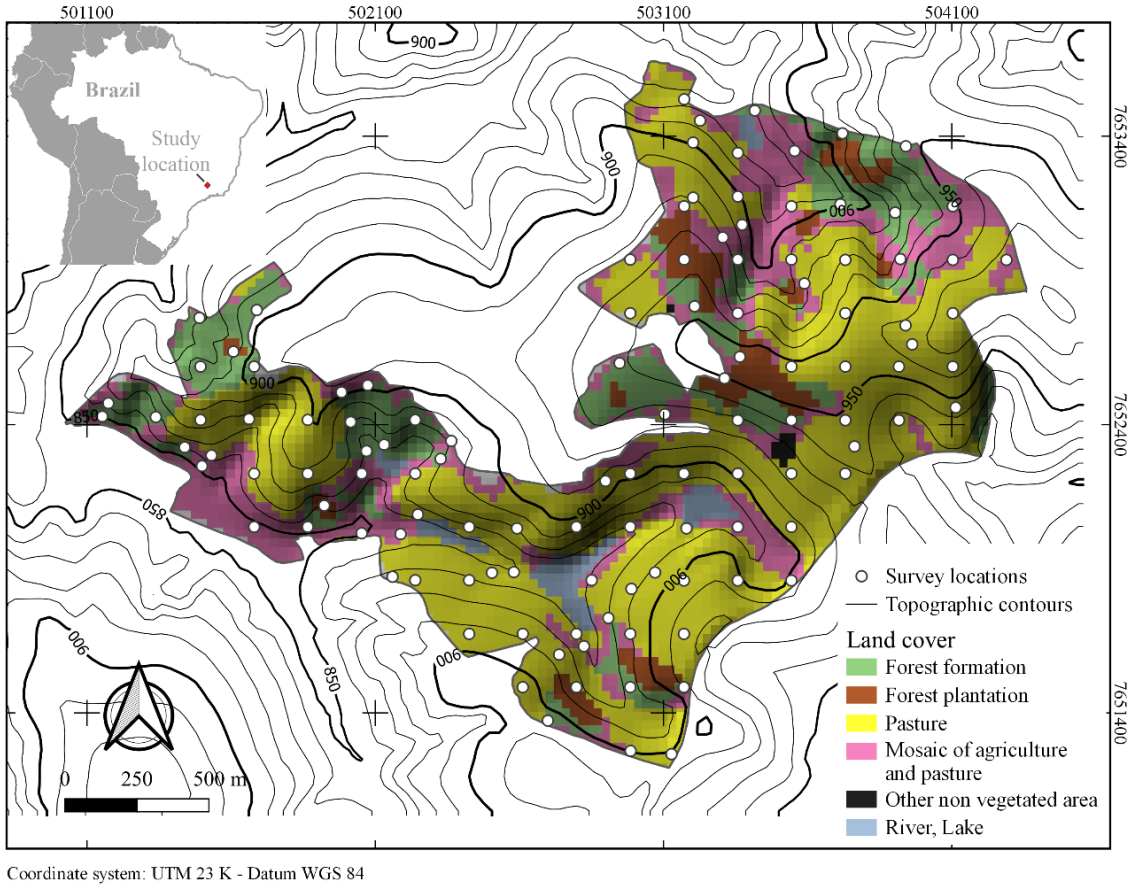

Figure 1. Study area location and land cover on the Campus of Federal University of Lavras, Southern Minas Gerais state, Brazil. Topographic contours interval is 10 m.

2.2. Vegetation greenness time-series and land surface phenology

All 168 scenes between 19-04-2013 and 12-08-2020 from the Landsat 8 OLI/TIRS sensors, path 218 row 75, of surface-reflectance imagery were queried in the earth engine database ("LANDSAT/LC08/C01/T1_SR" at code.earthengine.google.com), nevertheless, 17 scenes were not available. This image collection has been already atmospherically corrected and orthorectified, which improves its suitability for temporal analysis. Subsequently, the selected collection was cropped to the extent of the study area and the normalized difference vegetation index (NDVI), a proxy for vegetation greenness, was calculated and scaled by applying equation 1. Image cropping and NDVI calculation were realized using the raster package (Hijmans 2020) in the R platform (R-Core-team 2019).

Land surface phenology (LSP) metrics were derived by applying TIMESAT (Eklundh and Jönsson 2017), which is an algorithm developed for the extraction of seasonal parameters based on vegetation indices retrieved from optical remote sensing. Selection and fitting of seasonal models, chosen from asymmetric Gaussian functions, double logistic, and the Savitzky-Golay filter, was an iterative process involving visual interpretation and checking for reference values of NDVI in the literature (Jönsson and Eklundh 2004; Eklundh and Jönsson 2017). For that, the temporal stack of NDVI images was analyzed in TIMESAT.

$$NDVI = \frac{NIR - R}{NIR + R} \times 10^4 \quad (1)$$

Where NIR is near-infrared surface reflectance (band 5), and R is red surface reflectance (band 4). The 10^4 factor was applied for more efficient use of memory since a large quantity of image data was processed.

The main source of noise in the temporal signal of NDVI is caused by the occurrence of clouds and shadows, which generate a negatively biased noise (Hird and McDermid 2009). To coup with that, a weighted least-squares procedure is implemented sequentially in TIMESAT, giving more importance to high NDVI values in the time-series, building, as a result, a data 'upper envelope' upon the seasonal model is fitted model (Jönsson and Eklundh 2004; Eklundsh and Jönsson 2017). Landsat 8 scenes fully covered with clouds were treated as 'no data' when ingested into TIMESAT, as well as those corresponding with not available dates.

Thirteen LSP maps were derived for each season (Eklundh and Jönsson 2017; Jönsson and Eklundh 2004): time of the start of the season, time of the end of the season, length of the season, NDVI base level, time of the mid of the season, largest NDVI value for the fitted function, seasonal amplitude, rate of increase at the beginning of the season, rate of decrease

at the end of the season, large seasonal integral, small seasonal integral, NDVI value for the start of the season, and NDVI value for the end of the season. All LSP metrics were evaluated as soil covariates for the DSM.

2.3 Additional covariates

Soil forming-factor proxies depicting topography and soil parent material were also evaluated. For that, SAGA-GIS (Conrad et al. 2015) was used to derive terrain attributes commonly used in DSM applications based on a detailed digital elevation model (DEM) with a spatial resolution of 5 m, which was interpolated by the ANUDEM method from topographic contours of 1 m of vertical distance (Zheng et al. 2016). Besides elevation, terrain attributes included: slope, diffuse insolation, direct insolation, saga wetness index (SWI), stream power index (SPI), topographic position index (TPI), multiresolution valley bottom flatness (MRVBF), and multiresolution ridge top flatness index (MRRTF).

Parent material was interpreted from a magnetic susceptibility map obtained by Silva et al. (2016), which was derived from the analysis of B and C soil horizons of the same area (Curi et al. 2017). Subsequently, all soil covariates were aggregated to match the spatial resolution of the Landsat 8 data (30 m).

2.4 Rainfall seasonality

A rainfall time series was built from daily precipitation data from the 83687 BDMEP - INMET station, available at portal.inmet.gov.br. Daily data were aggregated to match the temporal resolution and the dates of the NDVI time-series, i.e. daily rainfall data was accumulated over 16-days periods (Figure 2). Analysis of the time-series of rainfall in TIMESAT allowed the definition of seven seasons, consequently, the initial image collection was filtered to match such periods.

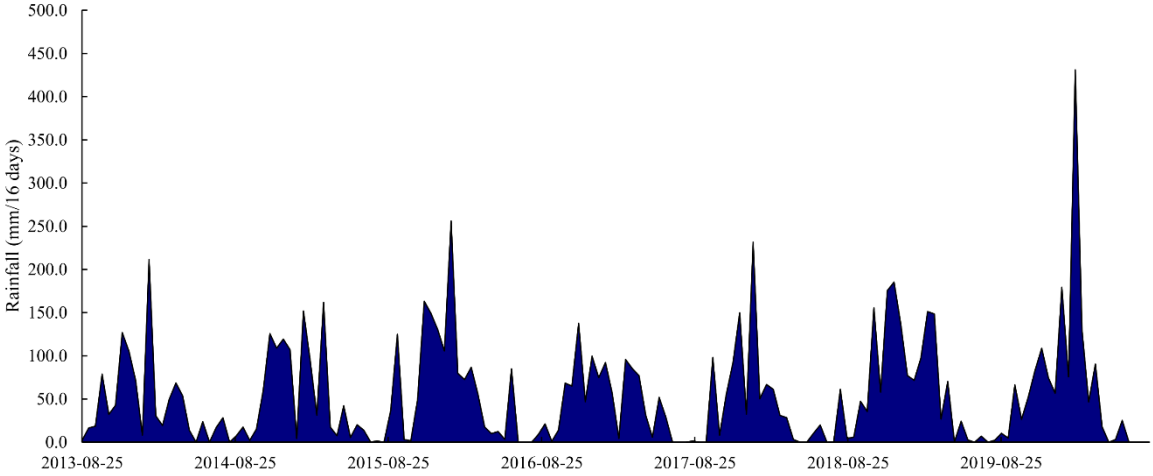

Figure 2. Time-series of aggregated 16-days rainfall for the study area: Campus of Federal University of Lavras, Southern Minas Gerais state, Brazil (date format: year-month-day).

Spearman's rank correlation analysis was performed between the large integrated NDVI (LI-NDVI) and the accumulated seasonal rainfall at each soil taxonomic class based on median values.

2.5 Digital soil mapping

Random forest (Breiman 2001; Liaw and Wiener 2002) was applied to associate spatial covariates to the occurrence of taxonomic soil classes. Soil survey revealed the occurrence of infrequent soil classes, given that modeling requires a minimum number of data, only soil classes with at least six records and under the same vegetation cover (pasture) were analyzed: Haplic Cambisol (HC), Red Latosol (RL), Red-Yellow Latosol (RYL), and Red-Yellow Argisol (RYA), which, in the Soil Taxonomy, corresponds to Typic Dystrudept, Rhodic Hapludox, Typic Hapludox, and Typic Hapludult, respectively (Soil Survey Staff 2014).

Accuracy assessment was evaluated on repeated 5-fold cross-validation, and random forest's variable importance, measured by the mean decrease in classification accuracy, was calculated globally and for each soil taxonomic class.

3. Results

3.1. Relationships between rainfall and vegetation greenness at each soil class

Spearman's rank correlation analysis between median values of the large integrated NDVI (LI - NDVI) and the accumulated seasonal rainfall is displayed in Table 1. The soil class that recorded the highest correlation between rainfall and LI – NDVI was the RL class (Rho = 0.7, $P < 0.05$).

Similar responses to rainfall are observed in the seasonal variation of RYL and RYA (Figure 3), which may be an effect of parent material, gneiss in both cases, differentiating from gabbro in the RL case (Curi et al. 2017). Soils developed from the same parent material usually present similar properties, as can be verified by their texture and soil organic matter (SOM) content (Figures 4 and 5), such a fact explains the similar behavior of these soils when evaluating the relationship between pasture productivity, interpreted as the large integrated NDVI metric (LI_NDVI), and rainfall.

Table 1. Spearman's rank correlation (Rho) between seasonal rainfall and large integrated NDVI for each soil taxonomic class.

STC	Rho	p-value
RYL	0.4	0.05
RYA	0.5	0.03
RL	0.7	0.02
HC	0.4	0.04

STC: Brazilian soil taxonomic class, RYL: Red-Yellow Latosol, RYA: Red-Yellow Argisol, RL: Red Latosol, HC: Haplic Cambisol.

High levels of SOM promote the retention and maintenance of water in the soil profile since it has a high association with chemical behavior and physical conditioning. Likewise, high clay content keeps water in the profile more easily, since the charges on the surface of the clays interact with the soil water. Although the clay content in the RL class is high when

compared to other soil classes (Figure 5), clay in this class is usually found in flocculated form, presenting microstructures that, due to their size, have a sandy behavior making infiltration efficient. Therefore, vegetation greenness on these soils may be more dependent on rainfall seasonality, as can be seen in Figure (3), in which the LI_NDVI curve of RL followed the rainfall seasonal pattern, which was corroborated by its highest correlation coefficient (Table 1).

Data obtained in previous studies using the integrated NDVI, interpreted as a proxy of seasonal productivity, indicated that there is an association among soil moisture, clay content, and natural fertility (Nicholson and Farrar 1994; Farrar, Nicholson, and Lare 1994). According to Araya *et al.* (2016), the vegetation productivity has a direct and proportional relationship with rainfall until it reaches a saturated condition; Figure 3 shows that there is a pattern depicting similar processes, notably for the class RL, which is characterized by a significant high clay content in the profile (Santos et al. 2018), enabling a differential response in plant water availability. It can be also observed that vegetation response depends on the accumulated seasonal rainfall on a yearly scale, notably for the season period 2017-2018 (Figure 3), which is the result of decreasing water input producing the expected theoretical pattern, i.e. the plant water availability conditioned by soil taxonomic class reached their maximum expression in the less water condition, this was also verified by Méndez-Barroso *et al.* (2009).

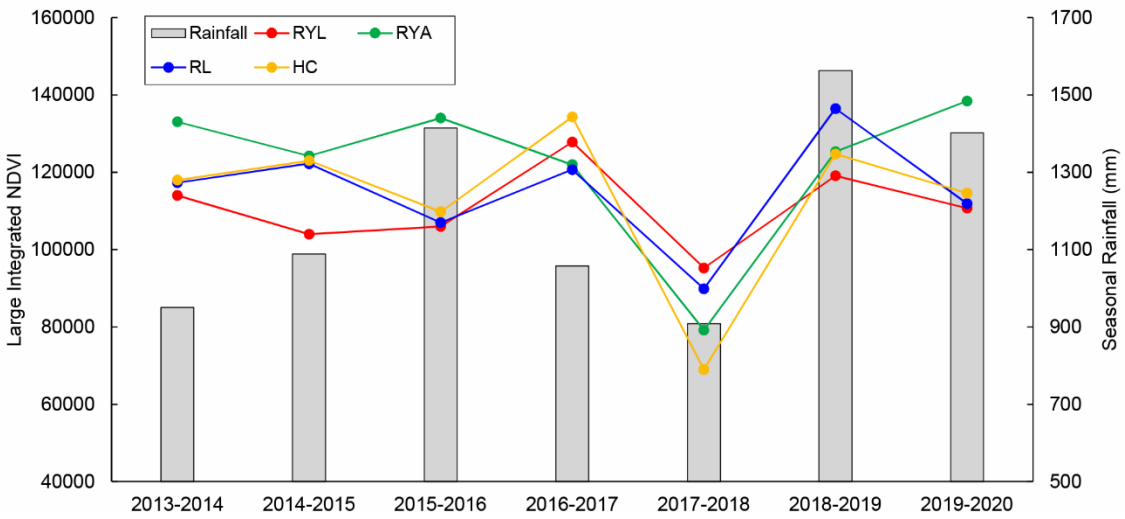

Figure 3. Rainfall seasonality and its relation with large integrated NDVI for each soil taxonomic class. RYL: Red-Yellow Latosol, RYA: Red-Yellow Argisol, RL: Red Latosol, HC: Haplic Cambisol.

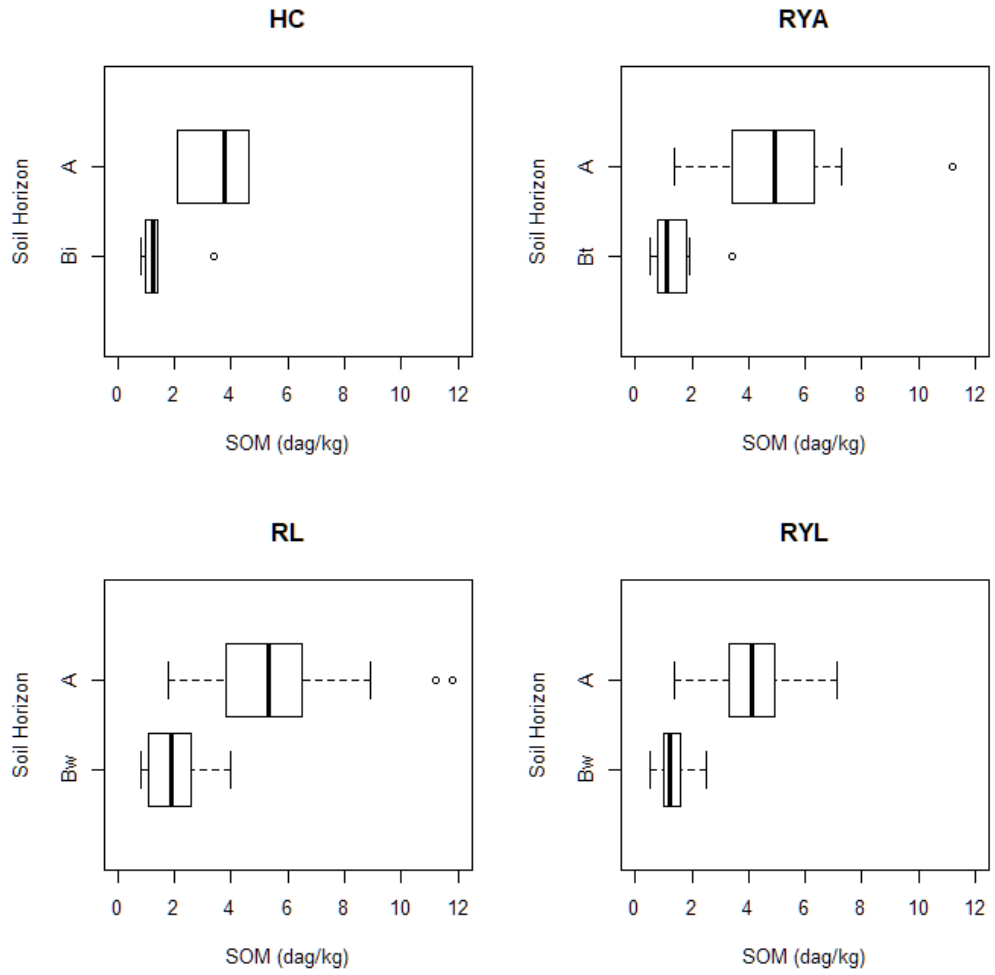

Figure 4. Soil organic matter (SOM) by soil taxonomic class and soil horizon. RYL: Red-Yellow Latosol, RYA: Red-Yellow Argisol, RL: Red Latosol, HC: Haplic Cambisol.

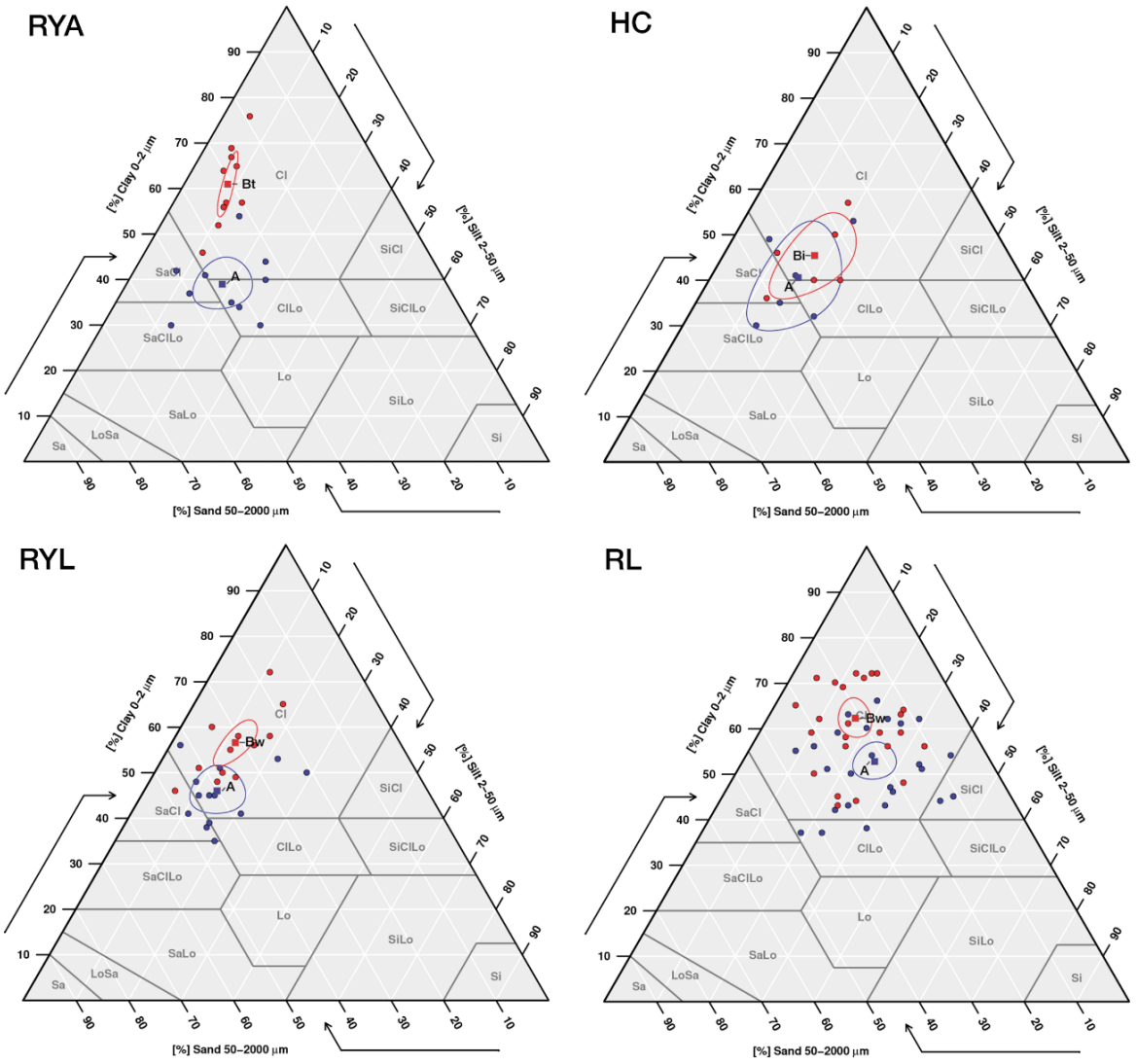

Figure 5. Soil texture class distribution (dots) and center confidence regions (90 % confidence) around centroids (squares) by soil horizon for each taxonomic class. RYA: Red-Yellow Argisol, HC: Haplic Cambisol RYL: Red-Yellow Latosol, RL: Red Latosol. Cl: clay, SiCl: silty clay, SaCl: sandy clay, ClLo: clay loam, SiClLo: silty clay loam, SaClLo: sandy clay loam, Lo: loam, SiLo: silty loam, SaLo: sandy loam, Si: silt, LoSa: loamy sand, Sa: sand.

3.2 Accuracy assessment and DSM

Performance of the use of LSP metrics in DSM recorded a median global accuracy of 61.1 % and a kappa value of 0.43, i.e. fair agreement (Landis and Koch 1977). Error rate was proportional to the occurrence frequency of the analyzed soil taxonomic classes, being lesser for the dominant classes: RL (12.1 %) and RYL (25.2 %), and higher for the less frequent classes: RYA (47.3 %) HC (87.3 %), imbalance in the dataset is still a challenging task in

DSM applications and the considerably low quantity of observations impeded the use of balancing techniques (Sharififar et al. 2019). The digital soil map in Figure 6 was filtered to show only the pasture vegetation cover (164.74 ha) and the geographic distribution of the analyzed soil taxonomic classes, which recorded the following area proportions: HC 10.09 ha (6.12 %), RL 83.95 ha (50.96 %), RYL 58.55 ha (35.54 %), and RYA 12.16 ha (7.38 %).

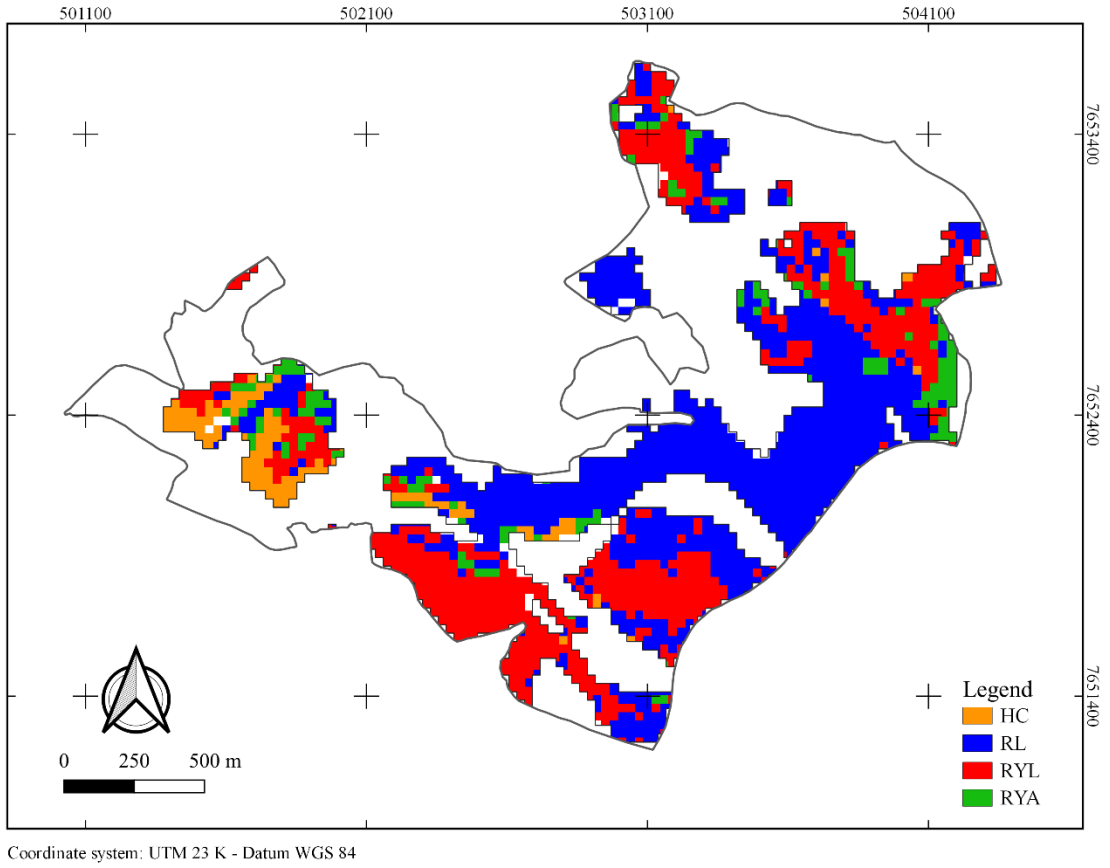

Figure 6. Digital soil map of soil taxonomic classes under pasture cover.on the Campus of Federal University of Lavras, Southern Minas Gerais state, Brazil. RYL: Red-Yellow Latosol, RYA: Red-Yellow Argisol, RL: Red Latosol, HC: Haplic Cambisol. Blank areas within the study area are vegetation covers dissimilar to pasture.

3.3. Covariates importance for DSM

Variable importance rank of the covariates evaluated for DSM is displayed in Figure 7 and the most important covariate maps in Figure 8. LSP metrics, notably LI - NDVI and base NDVI value of the seasons 2014 – 2015 and 2015 – 2016, recorded similar importance to those depicting parent material (magnetic susceptibility) and topography (CNBL). LI – NDVI,

which is the integral of the function spanning from start to the end of each season (Eklundh and Jönsson 2017), fitted by an asymmetric Gaussian function, is associated with seasonal vegetation productivity (Li et al. 2012; Araya et al. 2016; Nicholson and Farrar 1994). The base level, defined as the averaged fitted minimum values of NDVI has been already reported as an efficient DSM covariate (Yang et al. 2020) and reflects the soil condition over which vegetation cycles are driven.

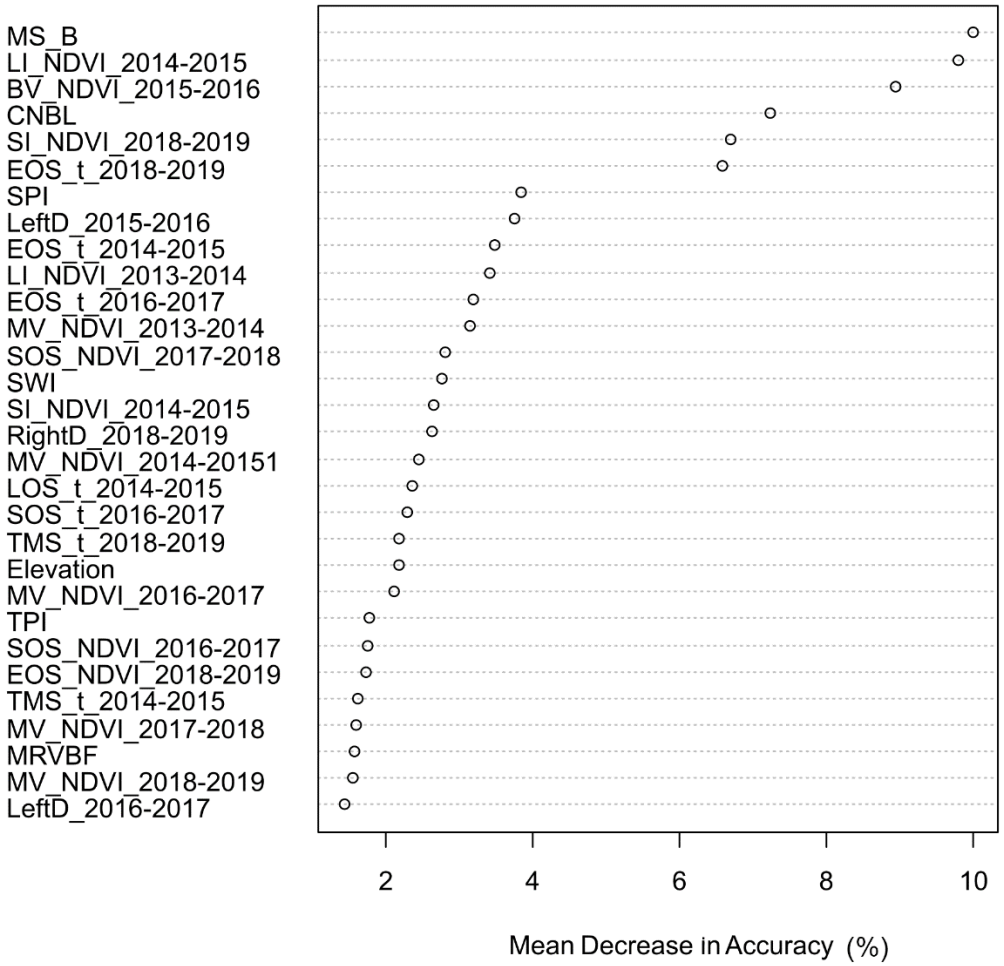

Figure 7. Random forest variable importance of the covariates assessed for the digital soil map. MS_B: Magnetic susceptibility of B horizons, CNBL: channel network base level, SPI: stream power index, SWI: saga wetness index, TPI: topographic position index, MRVBF: multiresolution valley bottom flatness, SOS_t: time for the start of the season, EOS_t: time for the end of the season, LOS_t: length of the season, BV_NDVI: base level value, TMS_t: time for the mid of the season, MV_NDVI: maximum value for the fitted function during the season, Amp_NDVI: seasonal amplitude, LeftD: rate of increase at the beginning of the

season (left derivative), RightD: rate of decrease at the end of the season (absolute value of right derivative), LI_NDVI: large seasonal integral, SI_NDVI: small seasonal integral, SOS_NDVI: value for the start of the season, EOS_NDVI: value for the end of the season.

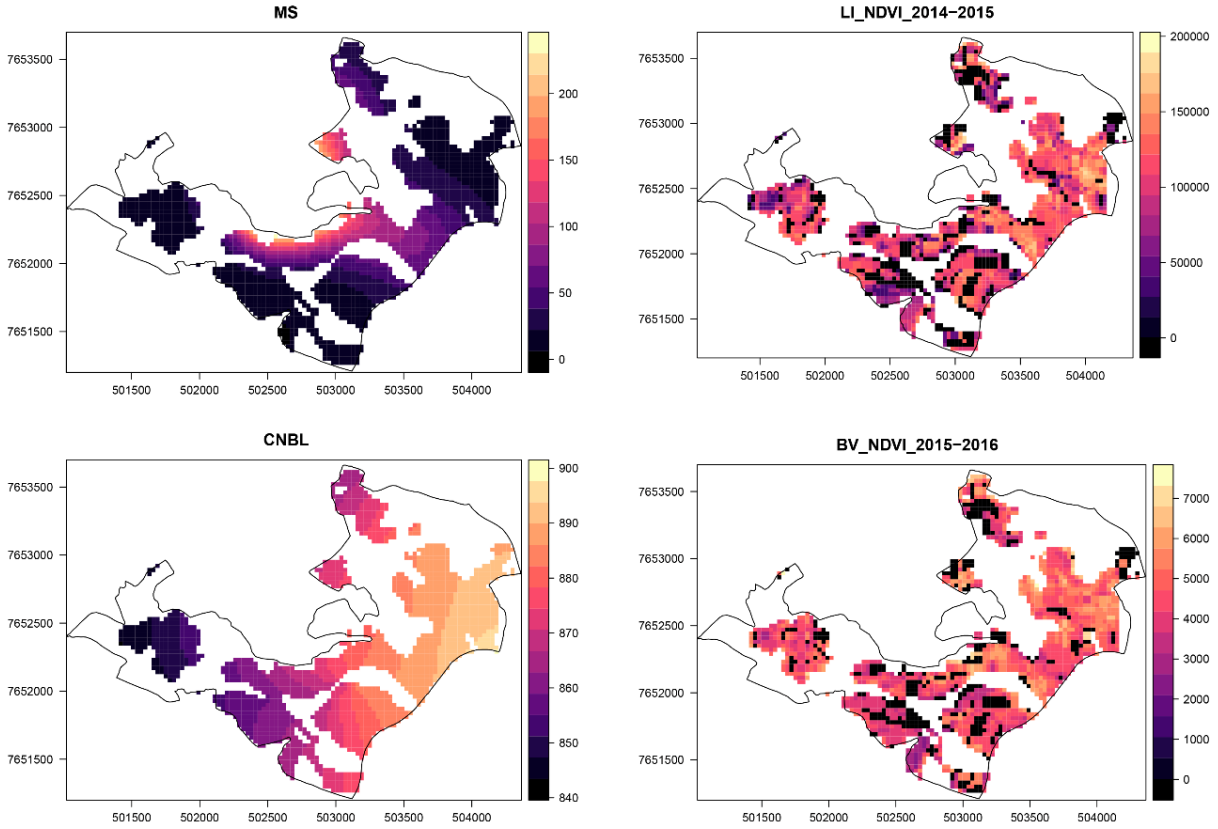

Figure 8. Random forest most important covariate maps: MS: Magnetic susceptibility of B horizons, CNBL: channel network base level, LI_NDVI: large seasonal integral, BV_NDVI: base level value. Black spots in LI and BV maps (below zero values) have insufficient data to fit a seasonal function.

4. Discussion

4.1. Soil control on the response of vegetation greenness to rainfall

Previous research has documented the effectiveness of temporal variability of vegetation greenness as a covariate for DSM of soil classes; Dematte *et al*. (2017), for example, reports that the analysis of NDVI seasonal difference can capture the control that soil exerts on vegetation greenness since soil pedological class reflect the water dynamics along the profile. Maynard and Levi (2017) also verified that soil acts as the main connector of vegetation and climate feedback. Those relationships support the use of vegetation temporal variability as a

DSM covariate. However, those studies have not included the temporal dimension of vegetation in an explicitly phenological sense, as is the case of this research, where the performance of time-synthetic images of NDVI phenological metrics and its relationship with seasonal rainfall as conditioned by soil taxonomic class was analyzed.

It was found that in all analyzed soil taxonomic classes, LSP metrics of NDVI of high importance for the discrimination of soil classes are related to the availability of water, remarkably in seasons with contrasting seasonal rainfall. These findings extend those of Maynard and Levi (2017), Araya *et al.* (2016), and Dematte *et al.* (2017), confirming that the vegetation greenness signal retrieved by remote sensing, is linked to water availability produced by the interaction of rainfall and soil condition on a phenological level and is also associated to preceding seasons. Additionally, the analysis of the effects of rainfall seasonality on the LI-NDVI metric validated their use in DSM, showing that rainfall acts as a ‘trigger' of the interactions of the soil-plant system.

4.2. Suitability of LSP data for DSM

Phenological synthetic imagery used as DSM covariate recorded similar importance than customary soil covariates and results provide interesting evidence for their application in digital mapping of soil taxonomic classes. However, some limitations are worth noting. Although the initial hypothesis was partially verified statistically, NDVI temporal signal may not reflect exclusively the effects of water availability, as indicated by Gholizadeh and Kopačková (2019), other factors, such as toxicity can act as vegetation ‘stressors’ and affect its spectral properties, as well as the interaction of soil fertility and taxonomic class (Demattê et al. 2017). Future work should therefore address the issue of functional signal filtering aiming at the elucidation of stronger temporal signatures.

5. Conclusions

The effects of soil taxonomic class on the response of vegetation greenness to rainfall were evaluated in a seasonal frame. It was verified that the temporal variability of vegetation greenness is conditioned by the soil in conjunction with rainfall seasonality. Seasonal dynamics of rainfall act as a 'trigger' for the soil-plant interaction, causing the most responsive temporal signature when transiting from a steady to a low-water input condition. While soil-forming factors depicting parent material and topography showed high importance for the classification and mapping of soil classes, LSP metrics related to the seasonal availability of water to plants, large integrated NDVI and NDVI base level, were also significantly important, remarkably for the Red Latosol class (Rhodic Hapludox). Results of the map production process support the use of vegetation seasonal metrics derived from remote sensing, in addition to other soil-forming factors, as a reliable source of information for the production of digital soil maps.

Acknowledgments

This study was financed in part by the Coordenação de Aperfeiçoamento de Pessoal de Nível Superior – Brasil (CAPES) – Finance Code 001, Conselho Nacional de Desenvolvimento Científico e Tecnológico (CNPq), and Fundação de Amparo à Pesquisa de Minas Gerais (FAPEMIG).

References

Alvares, Clayton Alcarde, José Luiz Stape, Paulo Cesar Sentelhas, José Leonardo de Moraes Gonçalves, and Gerd Sparovek. 2013. “Köppen’s Climate Classification Map for Brazil.” *Meteorologische Zeitschrift* 22 (6). Schweizerbart’sche Verlagsbuchhandlung: 711–728. doi:10.1127/0941-2948/2013/0507.

Araya, Sofanit, Greg Lyle, Megan Lewis, and Bertram Ostendorf. 2016. “Phenologic Metrics Derived from MODIS NDVI as Indicators for Plant Available Water-Holding Capacity.” *Ecological Indicators* 60 (January). Elsevier Ltd: 1263–1272. doi:10.1016/j.ecolind.2015.09.012.

Berry, Sandra L., and Brendan Mackey. 2018. “On Modelling the Relationship between Vegetation Greenness and Water Balance and Land Use Change.” *Scientific Reports* 8 (1): 9066. doi:10.1038/s41598-018-27139-0.

Breiman, Leo. 2001. “Random Forests.” *Machine Learning* 45 (1): 5–32. doi:10.1023/A:1010933404324.

Conrad, O, B Bechtel, M Bock, H Dietrich, E Fischer, L Gerlitz, J Wehberg, V Wichmann, and J. Böhner. 2015. “System for Automated Geoscientific Analyses (SAGA) v. 2.1.4.” *Geoscientific Model Develoment*, no. 8: 1991–2007. doi:10.5194/gmd-8-1991-2015.

Curi, N, SHG Silva, GC Poggere, and MD Menezes. 2017. *Mapeamento de Solos e Magnetismo No Campus Da UFLA Como Traçadores Ambientais*. 1st ed. Editora UFLA.

Demattê, José A.M., Veridiana Maria Sayão, Rodnei Rizzo, and Caio T. Fongaro. 2017. “Soil Class and Attribute Dynamics and Their Relationship with Natural Vegetation Based on Satellite Remote Sensing.” *Geoderma* 302 (March 2016). Elsevier: 39–51. doi:10.1016/j.geoderma.2017.04.019.

Dwyer, John L., David P. Roy, Brian Sauer, Calli B. Jenkerson, Hankui K. Zhang, and Leo Lymburner. 2018. “Analysis Ready Data: Enabling Analysis of the Landsat Archive.” *Remote Sensing* 10 (9): 1–19. doi:10.3390/rs10091363.

Eklundh, L, and P Jönsson. 2017. “Timesat - Software Manual.” Sweden: Lund and Malmö University. http://www.nateko.lu.se/TIMESAT/.

Farrar, T, S Nicholson, and A Lare. 1994. “The Influence of Soil Type on the Relationships between NDVI, Rainfall, and Soil Moisture in Semiarid Botswana. II. NDVI Response to Soil Moisture.” *Remote Sensing of Environment* 50 (2): 121–133. doi:10.1016/0034-

4257(94)90039-6.

Fathololoumi, Solmaz, Ali Reza Vaezi, Seyed Kazem Alavipanah, Ardavan Ghorbani, Daniel Saurette, and Asim Biswas. 2020. “Improved Digital Soil Mapping with Multitemporal Remotely Sensed Satellite Data Fusion: A Case Study in Iran.” *Science of The Total Environment* 721 (June). Elsevier B.V: 137703. doi:10.1016/j.scitotenv.2020.137703.

Fujii, Kazumichi, Makoto Shibata, Kaoru Kitajima, Tomoaki Ichie, Kanehiro Kitayama, and Benjamin L. Turner. 2018. “Plant–Soil Interactions Maintain Biodiversity and Functions of Tropical Forest Ecosystems.” *Ecological Research* 33 (1). Springer Japan: 149–160. doi:10.1007/s11284-017-1511-y.

Gholizadeh, A., and V. Kopačková. 2019. “Detecting Vegetation Stress as a Soil Contamination Proxy: A Review of Optical Proximal and Remote Sensing Techniques.” *International Journal of Environmental Science and Technology* 16 (5): 2511–2524. doi:10.1007/s13762-019-02310-w.

Helman, David. 2018. “Land Surface Phenology: What Do We Really ‘See’ from Space?” *Science of The Total Environment* 618 (March). Elsevier B.V.: 665–673. doi:10.1016/j.scitotenv.2017.07.237.

Hijmans, R.J. 2020. “Raster: Geographic Data Analysis and Modeling.” https://cran.r-project.org/package=raster.

Hird, Jennifer N., and Gregory J. McDermid. 2009. “Noise Reduction of NDVI Time Series: An Empirical Comparison of Selected Techniques.” *Remote Sensing of Environment* 113 (1). Elsevier Inc.: 248–258. doi:10.1016/j.rse.2008.09.003.

Jönsson, Per, and Lars Eklundh. 2004. “TIMESAT—a Program for Analyzing Time-Series of Satellite Sensor Data.” *Computers & Geosciences* 30 (8): 833–845. doi:10.1016/j.cageo.2004.05.006.

Landis, JR, and GG Koch. 1977. “The Measurement of Observer Agreement for Categorical Data.” *Biometrics* 33 (December). IEEE: 159–174. doi:10.1109/ICDMA.2010.328.

Li, Zhe, Ted Huffman, Aining Zhang, Fuqun Zhou, and Brian McConkey. 2012. “Spatially Locating Soil Classes within Complex Soil Polygons – Mapping Soil Capability for Agriculture in Saskatchewan Canada.” *Agriculture, Ecosystems & Environment* 152 (May). Elsevier B.V.: 59–67. doi:10.1016/j.agee.2012.02.007.

Liaw, Andy, and Matthew Wiener. 2002. “Classification and Regression by RandomForest.”

R News 2 (3): 18–22. doi:10.1159/000323281.

Ma, Yuxin, Budiman Minasny, Brendan P. Malone, and Alex B. Mcbratney. 2019. “Pedology and Digital Soil Mapping (DSM).” *European Journal of Soil Science* 70 (2): 216–235. doi:10.1111/ejss.12790.

Maynard, Jonathan J, and Matthew R Levi. 2017. “Hyper-Temporal Remote Sensing for Digital Soil Mapping: Characterizing Soil-Vegetation Response to Climatic Variability.” *Geoderma* 285 (January). Elsevier B.V.: 94–109. doi:10.1016/j.geoderma.2016.09.024.

McBratney, AB A.B, M.L Mendonça Santos, and B. Minasny. 2003. “On Digital Soil Mapping.” *Geoderma* 117 (1–2). Elsevier: 3–52. doi:10.1016/S0016-7061(03)00223-4.

Méndez-Barroso, Luis A., Enrique R. Vivoni, Christopher J. Watts, and Julio C. Rodríguez. 2009. “Seasonal and Interannual Relations between Precipitation, Surface Soil Moisture and Vegetation Dynamics in the North American Monsoon Region.” *Journal of Hydrology* 377 (1–2). Elsevier B.V.: 59–70. doi:10.1016/j.jhydrol.2009.08.009.

Mulder, V.L., S. de Bruin, M.E. Schaepman, and T.R. Mayr. 2011. “The Use of Remote Sensing in Soil and Terrain Mapping — A Review.” *Geoderma* 162 (1–2). Elsevier: 1–19. doi:10.1016/j.geoderma.2010.12.018.

Nicholson, S, and T Farrar. 1994. “The Influence of Soil Type on the Relationships between NDVI, Rainfall, and Soil Moisture in Semiarid Botswana. I. NDVI Response to Rainfall.” *Remote Sensing of Environment* 50 (2): 107–120. doi:10.1016/0034-4257(94)90038-8.

Padarian, J, B Minasny, and A.B. McBratney. 2015. “Using Google’s Cloud-Based Platform for Digital Soil Mapping.” *Computers & Geosciences* 83 (October). Elsevier: 80–88. doi:10.1016/j.cageo.2015.06.023.

R-Core-team. 2019. “R: A Language and Environment for Statistical Computing.” Vienna. www.R-project.org.

Rouse, JW, RH Jr Haas, JA Schell, and Deering DW. 1974. “Monitoring Vegetation Systems in the Great Plains with ERTS.” In *NASA SP-351, Third ERTS-1 Symposium*, 309–317.

Santos, H. G. dos, P. K. T. Jacomine, L. H. C. dos Anjos, V. A. de Oliveira, J. F. Lumbreras, M. R. Coelho, J. A. de Almeida, J. C. de Araujo Filho, J. B. de Oliveira, and T. J. F. Cunha. 2018. *Brazilian Soil Classification System*. 5th ed. Brasília, DF: Embrapa. https://www.embrapa.br/busca-de-publicacoes/-/publicacao/1094001/brazilian-soil-

classification-system.

Sharififar, Amin, Fereydoon Sarmadian, Brendan P. Malone, and Budiman Minasny. 2019. “Addressing the Issue of Digital Mapping of Soil Classes with Imbalanced Class Observations.” *Geoderma* 350 (October 2018): 84–92. doi:10.1016/j.geoderma.2019.05.016.

Silva, Sérgio, Giovana Poggere, Michele Menezes, Geila Carvalho, Luiz Guilherme, and Nilton Curi. 2016. “Proximal Sensing and Digital Terrain Models Applied to Digital Soil Mapping and Modeling of Brazilian Latosols (Oxisols).” *Remote Sensing* 8 (8): 614. doi:10.3390/rs8080614.

Soil-Survey-Staff. 2014. *Keys to Soil Taxonomy*. 12th ed. Washington, DC: USDA-Natural Resources Conservation Service. https://www.nrcs.usda.gov/wps/PA_NRCSConsumption/download?cid=stelprdb1252094&ext=pdf.

Souza, Carlos M., Julia Z. Shimbo, Marcos R. Rosa, Leandro L. Parente, Ane A. Alencar, Bernardo F. T. Rudorff, Heinrich Hasenack, et al. 2020. “Reconstructing Three Decades of Land Use and Land Cover Changes in Brazilian Biomes with Landsat Archive and Earth Engine.” *Remote Sensing* 12 (17): 2735. doi:10.3390/rs12172735.

Yang, Lin, Xianglin He, Feixue Shen, Chenghu Zhou, A-Xing Zhu, Bingbo Gao, Ziyue Chen, and Manchun Li. 2020. “Improving Prediction of Soil Organic Carbon Content in Croplands Using Phenological Parameters Extracted from NDVI Time Series Data.” *Soil and Tillage Research* 196 (October 2019). Elsevier: 104465. doi:10.1016/j.still.2019.104465.

Zheng, Xianwei, Hanjiang Xiong, Linwei Yue, and Jianya Gong. 2016. “An Improved ANUDEM Method Combining Topographic Correction and DEM Interpolation.” *Geocarto International* 31 (5): 492–505. doi:10.1080/10106049.2015.1059899.